

On the Paris coefficient and crack closure effects of Alporas aluminum foam

N. Geerlofs

December 2003

Master Thesis

Coaching:

Ir. C. van Kranenburg TNW-TM/MGM

Supervisor:

Dr. ir. J. Zuidema TNW-TM/MGM

Delft University of Technology
Department of Material Science
Rotterdamseweg 137
2628 AL Delft, The Netherlands

- 2 21 111

Bibliotheek Technische
Materiaalwetenschappen
Rotterdamseweg 137
2628 AL Delft

Abstract

Metal foams are a new class of materials with novel properties. Nowadays there is a number of commercial metal foams available. In the recent years a lot of effort has gone into research and development of metal foams. Most of the published literature is about the properties and behavior of specific metal foam.

The use of metal foam may well expand into more and new applications, where they are exposed to dynamic loads. The understanding of Fatigue Crack Growth is crucial in the design. It is therefore important to have a better understanding of their fatigue properties and fatigue behavior. At present the amount of work done on fatigue of metal foam has been mainly on S-N curves and hardly anything has been done on Fatigue Crack Growth.

Although Fatigue has many aspects, this work is aimed at crack growth in the Paris region. The Paris exponent and the occurrence of crack closure is of special interest. Based on published literature on other foams, the Paris exponent of metal foam is expected to be much higher than the common value of 2 up to 4 for solid metals. Crack closure has not been reported for metal foams. Since crack closure occurs in aluminum alloys it may well occur in aluminum based metal foams.

Fatigue Crack Growth experiments are used to investigate the Paris exponent and the crack closure. These experiments are performed on Alporas, which is a commercially available closed cell aluminum foam.

Properties of the metal foam as density, cell size, tensile strength and composition are determined to characterize the investigated metal foam. To complement the Fatigue Crack Growth experiments the failure behavior of the metal foam is studied by investigating the fracture surfaces with a Scanning Electron Microscope.

The Alporas foam is characterized as a closed cell foam made from a technical pure aluminum alloy. The foam has a relative density that is 9% of solid aluminum and has a cell diameter of 3.8 mm. This foam has a tensile yield stress of 1.4 MPa and a hardening exponent of 0.47. The composition of the aluminum from which the foam is made, is a technically pure aluminum with elements that were added during the foam production process.

The fatigue fracture surfaces show that the Alporas has a ductile and plastic failure mode.

The Alporas closed cell aluminum foam has a rather high Paris exponent of 15.6. The stable crack growth region or Paris region is from $\Delta K=0.095\text{MPa}\sqrt{\text{m}}$ up to $0.13\text{MPa}\sqrt{\text{m}}$. This range is very low and narrow compared to the normal range for solid metals. The material is less suitable for applications where failure predictions are necessary.

The Paris exponent is influenced by the free surface when the M(T)-sample thickness is below 35 mm. It was found that material variations are responsible for the spread in the experimental results. Also a micro-crack like inhibition effect was found at the low end of the Paris region.

A novel form of crack closure does occur in the Alporas aluminum foam during Fatigue Crack Growth. The behavior deviates from solid metals, because the

compressive fatigue loading is more effective. It is hypothesized that the structure of the foam transforms macro compression loads into surface tension loads on a micro scale. Thus enlarging the effective load available for Fatigue Crack Growth. This hypothesis needs verification.

An existing model for the Fatigue Crack Growth in metal foams has been verified. This *Beam Bending* model is based on material parameters. A good agreement between predicted values and experimental values was found.

A new model was developed to demonstrate the influence of the local structure on the Fatigue Crack Growth curves. This SCEF model has demonstrated the link between local foam structure and the bumpiness of Fatigue Crack Growth curves.

Contents

ABSTRACT	1
CONTENTS	3
LIST OF SYMBOLS	5
1 INTRODUCTION	7
2 METAL FOAMS; STRUCTURE AND MECHANICAL BEHAVIOR	9
2.1 STRUCTURE	9
2.2 MONOTONIC LOADING BEHAVIOR OF METAL FOAMS	9
2.3 FATIGUE BEHAVIOR OF ALUMINUM METAL FOAM	12
3 FATIGUE CRACK GROWTH	15
3.1 FCG CURVE STAGES	15
3.2 CRACK CLOSURE	16
3.3 INFLUENCES ON CRACK INITIATION	18
3.4 MODELS FOR FCG BEHAVIOR IN METAL FOAM	19
3.4.1 <i>Beam Bending model</i>	19
3.4.2 <i>Sequential Cell Edge Failure model</i>	22
4 EXPERIMENTAL DETAILS	25
4.1 MATERIAL DESCRIPTION	25
4.1.1 <i>Composition</i>	26
4.1.2 <i>Cell size</i>	27
4.1.3 <i>Density</i>	28
4.1.4 <i>Tensile strength and hardening exponent of Alporas foam</i>	28
4.1.5 <i>Hardness and grain size</i>	30
4.1.6 <i>Hardening exponent and tensile strength of AA1050</i>	30
4.2 FATIGUE CRACK GROWTH TESTING	31
4.2.1 <i>Sample geometry</i>	31
4.2.2 <i>Instrumental setup</i>	33
4.2.3 <i>Practices for FCG experiments</i>	37
4.2.4 <i>Data analysis</i>	38
4.3 SEM	39
5 RESULTS	41
5.1 FATIGUE CRACK GROWTH CURVE OF ALPORAS ALUMINUM FOAM	41
5.2 PARIS EXPONENT	43
5.3 CRACK CLOSURE	45
5.3.1 <i>Foam ΔK approach</i>	45
5.3.2 <i>ΔK approach according to ASTM</i>	46
5.4 FRACTURE SURFACES	49
6 DISCUSSION	55
6.1 FAILURE MODE	55
6.2 FATIGUE CRACK GROWTH CURVES	55
6.3 PARIS COEFFICIENT; EXPERIMENTAL AND LITERATURE	56
6.4 PARIS COEFFICIENT AND <i>BEAM BENDING</i> MODEL	57
6.5 FCG CURVE AND INFLUENCE OF STRUCTURE	59
6.6 COMPARISON OF THE CRACK CLOSURE FITS	60
6.7 LOAD MECHANISMS IN FOAM	61
6.8 CRACK CLOSURE FIT	61
6.9 HARDENING EXPONENT OF ALPORAS AND AA1050	62
7 CONCLUSIONS	63

REFERENCES	64
APPENDIX	67
APPENDIX 1: SETTINGS X-RAY SPECTROMETER	67
APPENDIX 2: COMPOSITION OF ALUMINUM ALLOY 1050.....	67
APPENDIX 3: SETTINGS OF HOWDEN PULSED D.C. CRACK LENGTH MEASURING SYSTEM	67
APPENDIX 4: PHYSICAL PROPERTIES; ALUMINUM ALLOY 1050	68
APPENDIX 5: PROPERTIES ALPORAS FOAM OF 11% DENSITY.	69

List of Symbols

α	Basquin exponent
α	ratio of the elliptical yield surface of the von Mises stress
β	Coffin-Manson exponent ($\beta=-c$)
ΔP	load difference
ΔK	difference in stress intensity factor
ΔK_{th}	stress intensity factor threshold value
ε_D	densification strain
σ_y	yield strength peak of foam
σ_{pl}	plateau stress of foam during compression
σ_{UTS}	ultimate tensile stress
ν_p	plastic Poisson ratio
(ρ^*/ρ)	density of foam relative to the density of solid aluminum
σ_{n-1}	standard deviation
a	crack length
A	Paris law constant
b	Basquin exponent ($\alpha=-b$)
c	Coffin-Manson exponent ($\beta=-c$)
C_1	constant derived from the Basquin law
C_2	constant derive from Coffin-Manson law
d	cell diameter
da/dN	Fatigue Crack Growth rate
E	Young's modulus
g_4	micro structural constant
g_5	micro structural constant
g_6	micro structural constant
H	sample height
HV	micro Vickers Hardness
K'	cyclic strength coefficient
K_c	critical stress intensity
K_{max}	maximum stress intensity
K_{min}	minimum stress intensity
l	cell wall length
m	Paris exponent
m^*	macro scale Paris exponent
n	strain hardening exponent
n'	cyclic strain hardening exponent
N_f	number of cycles to failure
P	load
P_{eff}	effective load
P_{max}	maximum load
P_{min}	minimum load
P_{OP}	counteracting force
r_y	size of a monotonic plastic zone
R	load ratio
S_v	surface area in unit volume

T	sample thickness
V _v	volume fraction in unit volume
U	crack closure effectiveness, optimized polynomial function
W	sample width
X	Howden signal

1 Introduction

Metal foams are a new class of materials with novel properties. They have a low density and novel physical, mechanical, thermal, electrical and acoustic properties. Metal foams can be made in a number of different processes from a wide range of metals and alloys. Nowadays there is a number of commercial metal foams available. Generally the aluminum based foams are produced using a melt route. Another process route is by using powder metal. In this process route a wide range of aluminum alloys can be used to make foam sandwiches.

The properties of metal foams are dependent on the material from which it has been made, the process by which it has been made, the characteristics of its cells and its density [1 and 2].

The following possible applications of metal foams are based on their novel properties:

- Lightweight structures like sandwich panels.
- Strain isolation, for example metal foams can take up the strain mismatch by crushing at a controlled pressure.
- Mechanical damping like mechanical vibration sound and shocks.
- Thermal management like heat exchangers, heat shields, and flame arrests.
- Filters.
- Electrodes.
- Catalyst carriers.

In the recent years a lot of effort has gone into research and development of metal foams. Most of the published literature is on the properties and behavior of specific metal foam [1 and 3].

The use of metal foam may well expand into more and new applications, where they are exposed to dynamic loads. The understanding of Fatigue Crack Growth is crucial in the design, especially in the aircraft and automotive industries. Therefore it is important to have a better understanding of their fatigue properties and fatigue behavior.

At present the amount of work done on fatigue of metal foam is mainly on S-N curves [4, 5, 6, 7, 8, 9, 10, 11, 12, 13 and 14] and hardly anything on Fatigue Crack Growth [15]. The literature on the Paris exponent for stable crack growth lists only very few polymer foams [13, 15,16 and 17] and even fewer metal foam materials.

Although fatigue has many aspects, this work is aimed at stable fatigue crack growth. This stage of crack growth is also known as the region of continuum behavior or the Paris region. In this work the Paris exponent and the occurrence of crack closure is of special interest.

Based on literature on other foams, the Paris exponent of metal foam is expected to be much higher than the common values for solid metals [13, 15, 16 and 17].

Although crack closure has not been reported for metal foams, it may well occur in aluminum based metal foams. Especially since crack closure is a common phenomenon in aluminum and its alloys [18].

In this work Fatigue Crack Growth experiments are performed on a commercial available closed cell aluminum foam [19 and 20]. The investigated metal foam is characterized. Properties of the metal foam as density, cell size, tensile strength and composition have been determined to characterize the investigated metal foam. The Fatigue Crack Growth experiments are the used means to investigate the Paris exponent and the crack closure.

To complement the Fatigue Crack Growth experiments the failure behavior of the metal foam has been studied by investigating the fracture surfaces with a Scanning Electron Microscope.

In literature several fatigue models are cited that might be applicable to Fatigue Crack Growth experiment on foam. These models are the *Micro mechanical* model [5], the *Beam Bending* model [17 and 21] and the *√area parameter* model [9 and 18]. Of these models only the *Beam Bending* model is used.

The *Beam Bending* model explains the Fatigue Crack Growth in the cellular structure of foam, based on the fatigue failure of foam structural elements.

Using the results of the Fatigue Crack Growth experiments, the *Beam Bending* model of J.S. Haung and S.Y. Liu [17] for the prediction of Fatigue Crack Growth in foams could be verified.

Based on the experience of the Fatigue Crack Growth experiments and the *Beam Bending* model, a new model has been developed. This model simulates the influence of the foam structure on the Fatigue Crack Growth and demonstrates the influence of the local structure on the experimental Fatigue Crack Growth curves.

2 Metal foams; structure and mechanical behavior

In this part the structure and mechanical behavior of metal foams is discussed. The characterization of a metal foam by the structure is explained in paragraph 2.1 The mechanical behavior of metal foam is explained in paragraph 2.2 for monotonic loading behavior and in paragraph 2.3 for fatigue behavior.

2.1 Structure

The metal foams consist of a three-dimensional cell structure. In open cells the cell walls are known as plateau borders or struts or cell edges. These connect in cell nodes to form a three-dimensional structure. In closed cells a membrane like face will seal off a cell from its neighbors [1, 2 and 16].

The structure of metal foam is characterized by:

- Cell topology, open or closed cells
- Relative density compared to the solid
- Cell size
- Cell shape

The material behavior is influenced by the structure. Other factors that influence the behavior are the homogeneity of the structure and anisotropy. The homogeneity influences the materials properties by deviations in local density and the influence of anisotropy is mainly due to the elliptical shape of the cells [8].

2.2 Monotonic loading behavior of metal foams

Aluminum metal foams behave ductile in compression. A typical compression stress strain curve as shown in figure 1 has four different regions [1 and 22]:

- The nominally linear deformation stage of the curve is where plastic deformation occurs at the cell nodes. The load on a cell face or cell wall due to the deformation causes the cell node to form a plastic hinge at the cell node [3]. Deformation of closed cell foams introduces a tensile stress in the cell face or membrane. This stretching increases the macroscopic stiffness and strength. In this region the Poisson ratio of the foam (ν_p) is about 0.33 [22 and 23].
- The non-linear deformation stage where the slope of the initial loading curve is reduced due to a strain hardening effect. This is due to localized plasticity in the sample well below the compressive strength of the foam. The deformation takes place by plastically buckling or bending membranes or cell edges [22, 23 and 24].
- In constant stress plateau the cell edges yield in bending, while the stress strain curve remains constant or gently rises. In open cell foam uniform strain develops throughout the material which compresses uniformly. In closed cell foam the foam suffers local plastic deformation that develops into bands of crushed cells. The initiation of the first cell band collapse is reflected by the peak of the yield strength σ_y . A crushed band first forms at the weakest section of the foam, where the average normal strain increases to a saturation value of about 30% of the nominal strain. As the loading increases the previously formed bands harden, giving rise to new bands in neighboring regions. In the constant stress plateau the

plastic Poisson ratio is very small ($\nu_p \approx 0$). The cells outside the deformation bands deform elastically and retain their original shape.

- **Densification;** The foam crushes at a plateau stress σ_{p1} until the densification stage sets in. The beginning of this densification stage is marked by densification strain ε_D , where the foam is crushed until opposing cell faces touch and the stress strain curve rises steeply. The compression for both open cell foam and closed cell foam is uniform and the densification strain, ε_D , can be as high as 60%.

In tension the failure behavior of foam is more brittle than compression loading. The tensile curve is composed of the first two stages from the compression curve, notably the nominally linear deformation stage and non-linear deformation stage. The material fails at the end of the second stage. Failure strains are in the range of 0.2 to 2.0% [1 and 4]. The difference between tension and compression yield strengths is about 10%.

Crack growth

The crack initiates at defects either in the cell walls or at the surface. The crack propagates through cell walls as plane stress cracks in the thin sheets [3 and 25]. The crack meanders across the adjoining walls and progresses through the material, generally as one distinct entity with occasional branches [25 and 26].

The cracks will grow via prior defects in the cell walls. Micro cracks form near the crack tip, at the maximum load. In the wake of the advancing crack tip a crack bridging zone can develop. In general the deformation is localized in parts of only a few cell walls.

The energy dissipated upon crack growth arises from cell wall necking and is determined by the plastic stretch that occurs over the necking zone [24 and 27]. This plastic zone is localized in a narrow strip ahead of the crack tip and has a height of the order of the wall thickness. This mechanism is facilitated by necking of cell walls followed by nucleation, growth and coalescence of voids. Necking of the cell walls is due to plastic deformation before fracture [4 and 28].

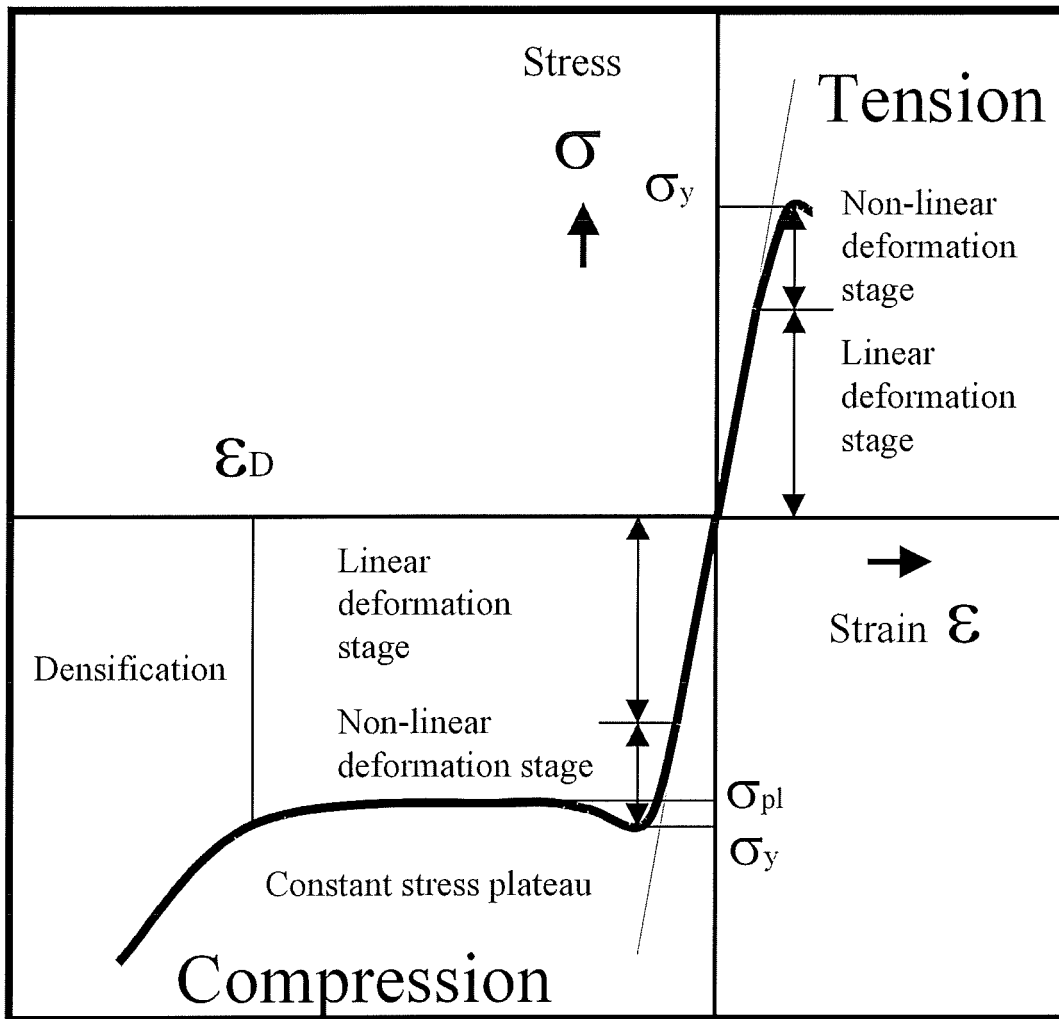


Figure 1 Tensile and compression curve of metal foam, different stages.

2.3 Fatigue behavior of aluminum metal foam

At a load level near the yield strength, a metal foam will gradually and progressively deform under cyclic load [1 and 4]. The cell walls progressively straighten under a tensile mean stress and progressively bend under a compressive mean stress. In cyclic loading with alternating compressive and tensile loads, the tensile load behavior is dominant. Generally this leads to a brittle fracture due to the tensile load.

The cell faces in a closed cell foam are subjected to a tensile stress when the cell edges bend, see figure 2. Consequently cracks initiate and grow in the weaker cell faces and then progress into the cell edges [1, 6, 7 and 8]. The formation of cracks causes softening of the material. A fatigue crack will develop at the weakest sites in the material. This results in a rough fracture surface where the crack switches between cells at different levels. The failed cell edges show necking, plastic deformation and voids.

Samples tested at a stress lower than the fatigue limit suffers only a negligible amount of plastic deformation. At these conditions there is no cracking or bending of the cell edges [5].

Foams have a very high Fatigue Crack Growth rate. This is shown by the values of the Paris exponent m , quoted in the literature [13, 15, 16 and 17], see table 1. This Paris exponent characterizes the speed with which a crack will increase in the stable crack growth region (II) of the Paris curve, see paragraph 3.1.

Table 1: Materials with a high Paris exponents.

Material	Paris exponent m	Remark Note R is load ratio	Reference
Alporas (Al foam)	25	R= 0.1, CT sample	[15]
Alulight (Al foam)	20	R= 0.1, CT sample	[15]
Phenolic foam	13	R= 0.2, CT sample	[17 and 16]
Polyurethane foam	10	-	[17 and 16]
PVC foam	7.5	R= 0.1 CT sample	[13]
Polymethacrylimide foam	17.3	R= 0.1 CT sample	[13]
Powder metal, steel	10 to 18	R= 0.1, 0.8, 3 point bending	[29]
Polyisocyanurate foam	15	-	[16 and 17]

Deformation of a schematic hexagonal closed cell

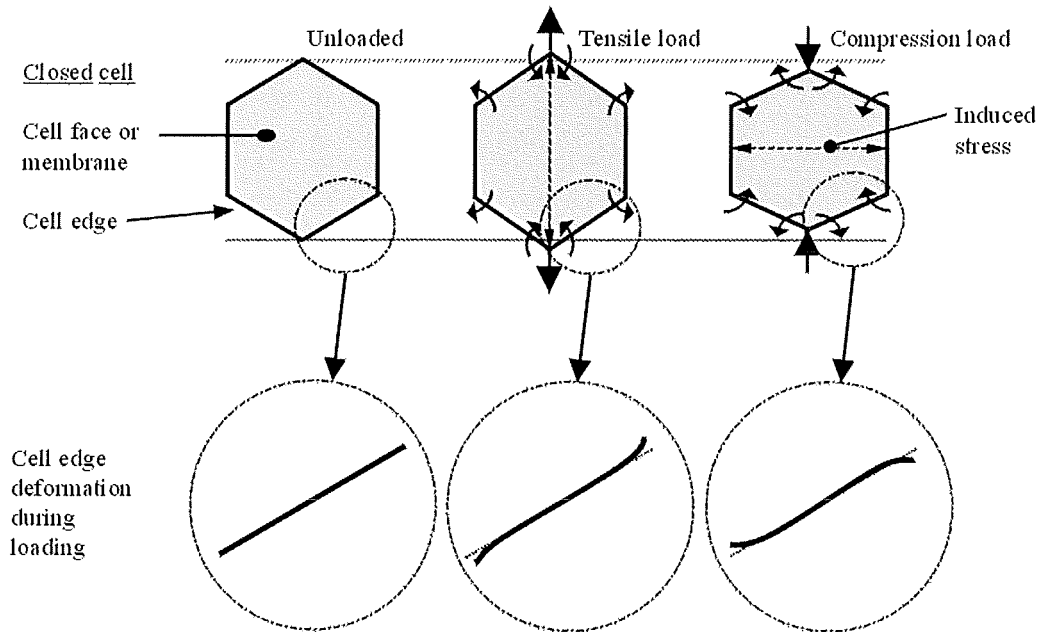


Figure 2 Deformation of a closed cell

3 Fatigue Crack Growth

The part of the Fatigue Crack Growth (FCG) curves that is essential for the determining of the Paris exponent and the occurrence of crack closure are explained in paragraph 3.1. The phenomenon of crack closure itself is explained in paragraph 3.2.

The effect of stress-strain fields at notches is explained in paragraph 3.3, since it is possible that similar effects can be encountered in metal foams during FCG experiments.

3.1 FCG curve stages

When a sample is subjected to a cyclic load, cracks can initiate or grow from an existing crack nucleus to macroscopic size and finally lead to failure. The characteristic shape of the FCG curve $da/dN - \Delta K$ is divided into three regions according to the curve shape mechanisms of crack extension and various influences on the curve, see figure 3 [18 and 30]:

- In region I the crack initiation takes place. This region is characterized by the threshold value ΔK_{th} below which cracks do not propagate or propagate extremely slow. In this region the behavior is influenced by the structure of the material. So the material has a non-continuum behavior. This region is absent in cases with existing flaws of sufficient size [31].
- In region II the crack growth rate often displays a linear relation between $\log(da/dN) - \log(\Delta K)$. A macro crack has dimensions sufficient for its growth to depend only on bulk properties and non-local conditions rather than local ones. In Linear Elastic Fracture Mechanics (LEFM) terms this means that macro crack growth can be described by the stress intensity factor concept [18]. Note. The stress intensity factor K is a continuum value. In this the region the material has a continuum behavior. This region of stable crack growth is important in the calculation of the time it takes a crack to grow from a certain initial size to the maximum permissible size.
- Region III is a region of accelerated crack growth or unstable crack growth. The material will fail when K_{max} exceeds the fracture toughness K_c .

In region II the linear relationship between $\log(da/dN) - \log(\Delta K)$ is described by the empirical relation of the Paris Law:

$$\frac{da}{dN} = A \left(\Delta K_I \right)^m \quad (1)$$

In this da/dN is the crack growth per cycle, A is the Paris law constant, m is the Paris exponent and ΔK is the difference in stress intensity factor at maximum and minimum stress. The Paris exponent m has a value of 2 to 4 for solid metals, but much higher values for foam, see paragraph 2.3.

In solids it is assumed that the crack does not grow during the compression part of the load cycle time. That is why only the positive part of the load is thought to have an effect on the crack growth, in solid metals. Therefore ASTM E 647-00 [32] prescribes the use of $\Delta P = P_{max}$ at load ratios of $R \leq 0$ for determining ΔK .

In foams both a compression load and a tensile load deform the material in bending [16], see figure 2. In this thesis it is assumed that both positive and negative parts of the load have an influence on the FCG. For this reason $\Delta P = P_{max} - P_{min}$ is used instead for determining ΔK , at load ratios $-1 \leq R \leq 1$.

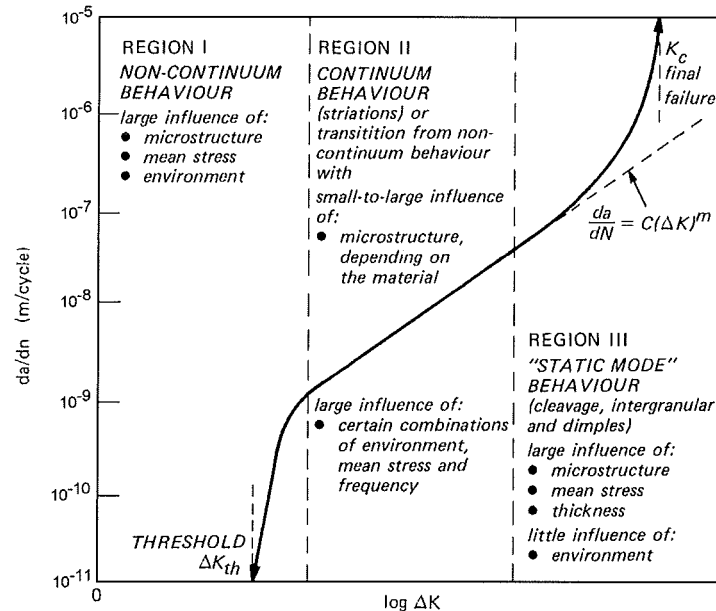


Figure 3 Schematic Fatigue Crack Growth (FCG) curve, [18]

3.2 Crack closure

Crack closure is a phenomenon where a process creates an extra space volume material at the fracture surface near the crack tip, during crack formation. This extra volume prevents the crack from closing in an unloaded state and acts like a force that partially counteracts the minimum load, see figure 4. For this reason the effected ΔK on the crack is smaller than the load from the externally applied load, $P_{eff} = P - P_{OP}$. This effect has a greater influence at lower values of load ratio R . This is the reason why the FCG curve shifts with the load ratio R .

Causes of crack closure can be:

- Plastic deformation in the crack flanks that resist closure of the crack
- Oxide or particles in the crack tip
- Coarse crack surfaces
- Phase changes in the crack surfaces

In plasticity induced crack closure a plastic zone is created at the tip of the crack, each time the loading increases [18]. Also a smaller reversed plastic zone is created during unloading. This plastic zone leaves a residual plastic deformation in the wake of the growing crack. Due to this a counteracting force will develop during the closing of the crack, see figure 4.

The size of a monotonic plastic zone r_y is given by:

$$2r_y = \frac{1}{\pi} \left(\frac{K_{MAX}}{\sigma_Y} \right)^2 \quad (2)$$

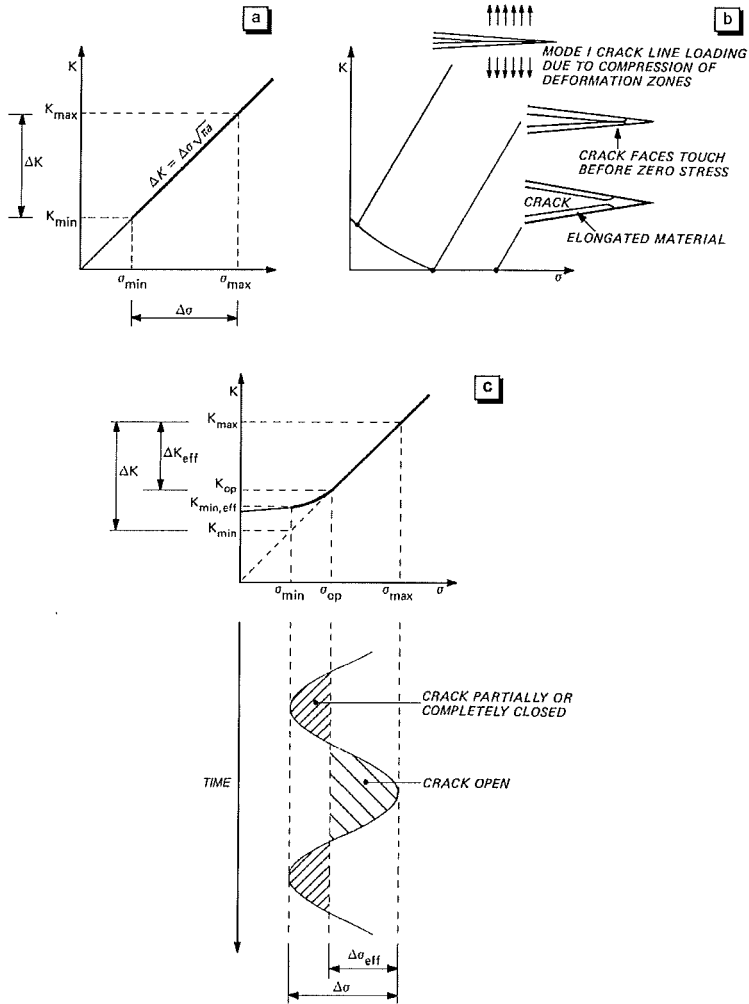


Figure 4: Crack closure [18]

3.3 Influences on crack initiation

Cracks initiate at the surface due to roughness or scratches. Another possibility for crack initiation is in the bulk of the material, where precipitates, inclusions or other stress concentrators can lead to crack initiations.

In the presence of a stress concentrator it is possible that the crack growth begins under conditions of local plasticity [18]. The crack starts to grow through the stress strain field of the stress concentrator before it reaches the stress strain field of the bulk material, see figure 5.

There are three situations where the FCG curve deviates from the normal da/dN versus ΔK curve:

- In plastic stress strain fields the plastic strain range controls the growth. The initial crack growth rate is high, but diminishes rapidly with the plastic strain range.
- In elastic stress strain fields a deviation is due to the fact that short cracks tend to grow faster than long cracks.
- A combination of both effects.

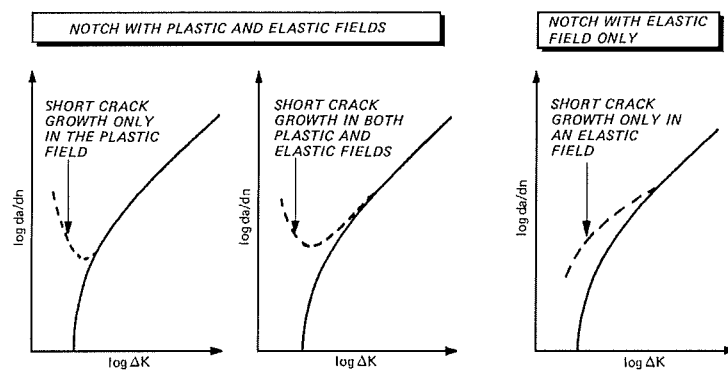


Figure 5: Influences on crack initiation [18]

3.4 Models for FCG behavior in metal foam

The following models that are found in literature [3] might be useful for foams:

- Micro mechanical model [5]; This is a model for predicting the fatigue life of foam under compression/compression or tension/tension loading. This is a modified creep model of Gibson and Ashby [16], which is based on power law creep.
- *Beam Bending* model [17 and 21]; This model describes the fatigue macro crack propagation of cellular materials.
- $\sqrt{\text{area}}$ parameter model [9 and 18]; This is an empirical model that predicts the fatigue limits on the basis of the maximum defect size and the Vickers hardness.

From these models only the *Beam Bending* model is suitable for modeling FCG experiments. This model is explained in paragraph 3.4.1.

A newly developed Sequential Cell Edge Failure (SCEF) model which is based on the experience of the FCG experiments and the *Beam Bending* model, is explained in paragraph 3.4.2.

3.4.1 *Beam Bending* model

The *Beam Bending* model of J.S. Haung and S.Y. Liu [17] is a fatigue model for open cell foam. The model was originally developed for hexagonal honeycomb and was later adapted for open cell foams. This model is also applicable to closed cell foams when the thickness of the cell faces is small compared to the thickness of the cell edges.

In this model the first unbroken cell edge in front of the crack tip is subjected to a cyclic bending load. The cyclic axial load on the material results in a cyclic bending load on the cell edges, see figure 2. This induced load is not enough to induce direct failure. Crack growth will start at the existing defects in the first unbroken cell edge in front of the crack tip. The crack growth in the cell edge follows the Paris equation. The stress intensity factor in the bending cell edge is approximated by the stress intensity factor of a supported strut in three point bending, where the cell thickness is much smaller than its length. It is assumed that the cell edge will fail at a crack length that is small compared to its thickness.

When the cell edge fails the macro crack will be increased by the cell cross section. In other words the crack growth rate is determined by the cell size and the number of cycles it takes to fail that cell edge.

This model gives the following equation for the macro FCG rate [17]:

$$\left(\frac{da}{dN}\right)^* = A^* (\Delta K_I^*)^{m^*} = \frac{l}{N_f} = g_4 A l (m-2) a^{(m/2)-1} \left[\frac{1}{\sqrt{l}} \left(\frac{\rho^*}{\rho} \right)^{-3/2} \right]^m (\Delta K_I^*)^m \quad (3)$$

In this equation l is the cell wall length, N_f is the number of cycles to failure, m is the Paris exponent, g_4 is a micro structural constant, a is the crack length and (ρ^*/ρ) is the density of the foam relative to the density of solid aluminum. Parameters marked with * are macro scale parameters.

In this equation the macro scale Paris exponent m^* is equal to m .

For foams the following equation can be derived for high cycle fatigue, using Basquin's law.

$$\left(\frac{da}{dN}\right)^* = \frac{l}{N_f} = A^* (\Delta K_I^*)^{m^*} = g_5 l \left[\frac{1}{C_1 \sqrt{\pi l}} \left(\frac{\rho^*}{\rho}\right)^{-3/2} \right]^{1/\alpha} (\Delta K_I^*)^{1/\alpha} \quad (4)$$

In this g_5 is again a micro structural constant and α ($\alpha=-b$) is the Basquin exponent. Some values of the Basquin exponent are given in table 2. The macro scale Paris exponent m^* is equal to α^{-1} . Note $m^* = \alpha^{-1}$ is only valid for situations where ΔK is constant and is not valid for materials as solid metals.

In this formula (4) C_1 is a constant derived from the Basquin law:

$$C_1 = \Delta \sigma (N_f)^\alpha \quad (5)$$

Table 2: Literature values of Basquin exponent of solid metals.

Material	Basquin exponent α ($\alpha=-b$)	Paris exponent: <i>Beam Bending</i> model, high cycle fatigue model $m^* = \alpha^{-1}$.
All metals	0.05 – 0.12 [30]	8.333 - 20
All metals	0.067 – 0.125 [5]	8 - 15
Some aluminum alloys	0.106 – 0.126 [33]	7.9 - 9.43
AA1100, annealed	0.106 [33]	7.5
AA2014, T6	0.106 [33 and 36]	7.5
AA2024, T4	0.11 [36]	9.1
AA2024, T351	0.124 [33]	8.1
AA5456, H31/H311	0.11 [33 and 36]	9.1
AA7075, T6	0.126 [33 and 36]	7.9

In low cycle fatigue the stresses will be higher. There will be plastic deformation in the cell edges. In this range the Coffin-Manson law is used to derive the following equation:

$$\frac{da^*}{dN^*} = \frac{l}{N_f} = g_6 l \left[\frac{1}{C_2 K' \sqrt{\pi l}} \left(\frac{\rho^*}{\rho}\right)^{-3/2} \right]^{1/n'\beta} (\Delta K_I^*)^{1/n'\beta} = A^* (\Delta K_I^*)^{m^*} \quad (6)$$

In this g_6 is again a micro structural constant, n' is the cyclic strain hardening exponent, K' is the cyclic strength coefficient and β is the Coffin-Manson exponent ($\beta=-c$). Some values of the Coffin-Manson exponent are given in table 3. The macro scale Paris exponent m^* is equal to $(n\beta)^{-1}$. In this formula C_2 is a constant derived from Coffin-Manson law:

$$C_2 = \Delta \varepsilon^{pf} (N_f)^\beta = 2^{\beta-1} \Delta \varepsilon_{pf} \quad (7)$$

For high cycle fatigue this model is reported [17] to give good results for polyisocyanurate foam, phenolic foam and polyurethane foam, but it has not been applied to aluminum foam. Validation of the *Beam Bending* model is therefore required.

Table 3: Literature values of Coffin-Manson exponent

Material	Coffin-Manson exponent c ($\beta=-c$)	n' (n_f) cyclic strain hardening exponent	Paris exponent: <i>Beam Bending</i> model, model low cycle fatigue, $m^*=(n'\beta)^{-1}$	n strain hardening exponent
Aluminum	0.61 [34]	0.093 [34]	17.6	-
AA1050, annealed	-	-	-	0.388 (at 50 °C) [35]
AA1100, annealed	0.69 [33]	-		
AA2014, T6	0.65 [33 and 36]	0.16 [36]	9.6	-
AA2024, T4	0.59 [33] 0.52 [36]	0.08 [36]	21 24	0.20 [36]
AA2024, T351	-	0.09 [33]	-	-
AA5456, H311	0.67 [33 and 36]	0.16 [36]	9.3	-
AA6061, H651	-	0.10 [33]	-	
AA7075, T6	0.52 [33 and 36]	0.10 [33] 0.146 [36]	19.2 13.2	- 0.113 [36]
Most solid materials	0.5 - 0.7 [30]	0.1 to 0.2 [30]	7 to 20	0.1 to 0.5 [30]

3.4.2 Sequential Cell Edge Failure model

The Sequential Cell Edge Failure model (SCEF) describes the failure of metal foam during fatigue. It is assumed that the foam will fail in the weakest place at the crack front. This place will usually have the lowest local density, which will make the local stress the highest at this place. Due to the fact that the number of cycles to failure in a S-N curve is on a logarithmic scale, a failure on the weakest place will hardly affect the fatigue life in other places.

After failure the fatigue process will move to the next weakest place at the crack front and so on. In this way the fatigue process of metal foam can be viewed as a number of sequential fatigue processes.

Closed cell foam consists of cell edges and membrane like cell faces. Most of the metal content is in the cell edges [26]. The influence of the relatively thin cell walls on the fatigue life can be neglected. So the fatigue process can be approximated by sequentially subjecting cell edges to the fatigue. It is assumed that the Fatigue Crack Growth in the cell edge is described by the Paris equation.

The macro crack length in the M(T) sample determines the ΔK to which a cell edge is subjected. During the Fatigue Crack Growth in one of the cell edges, the ΔK is approximated as being constant. After failure of the cell edge the macro crack grows with the area of the cell cross section. This area is divided by the total crack front and increases the average macro crack length and therefore increases the ΔK . This requires a more or less straight crack front.

The macro crack growth rate is the macro crack growth due to the failure of one cell divided by the number of load cycles that were needed for this failure.

Sequential Cell Edge Failure Model

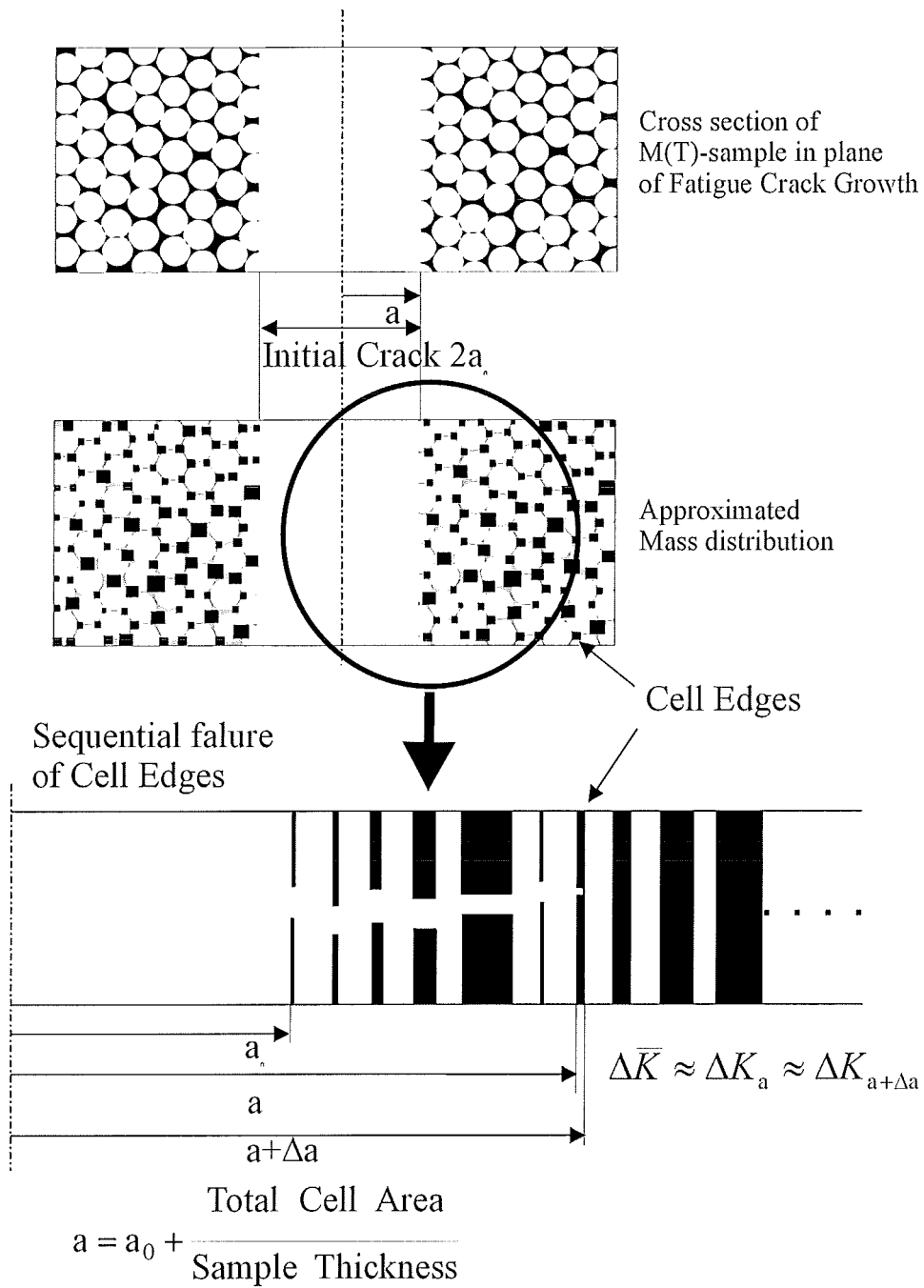


Figure 6 *Sequential Cell Edge Failure* model

4 Experimental details

The material that has been tested and the way those tests have been performed are discussed in this part. In paragraph 4.1 the aluminum foam is characterized by determining the chemical composition and properties as density, cell size, hardness and tensile strength. This is done to establish what kind of metal foam is investigated. In paragraph 4.2 the setup and protocols by which the FCG experiments are performed are explained. In paragraph 4.3 the investigation of the fracture surfaces is discussed.

4.1 Material description

In this investigation the commercial available aluminum foam *Alporas* was used. This material is made and marketed by Shinko Wire in Japan. Alporas is closed cell foam with a density relative to solid pure aluminum of approximately 9%. In literature a cell diameter of 4.5 mm [19] is given. The material was ordered and received in plates of 600*400*40 mm.

Alporas is made by stabilizing bubbles in molten aluminum [37]. To stabilize the melt the viscosity is increased by stirring 1.5wt% Ca into the melt. This is done for 6 minutes in an ambient atmosphere. The blowing agent of 1.6wt% TiH₂ is added to the melt in the casting mold. After stirring the molten material expands to fill the mold. After 15 minutes curing a fan is used to cool the foamed material. The cast material is 450*2050*650 mm and typically weights 160kg.

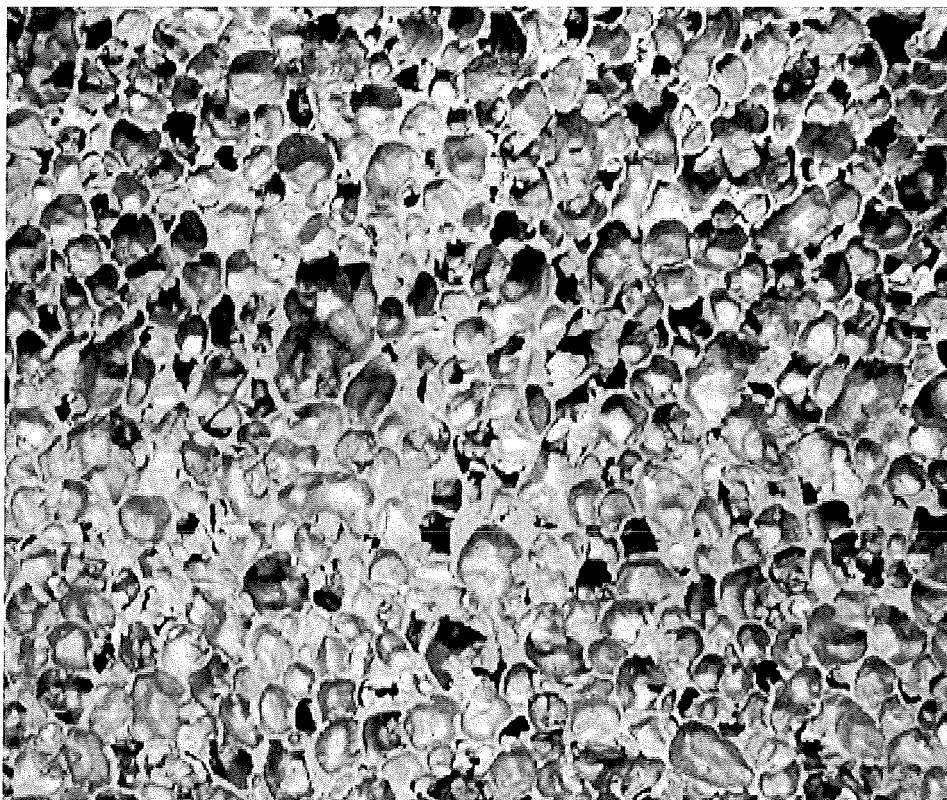


Figure 7 Structure of Alporas closed cell aluminum foam.

4.1.1 Composition

The composition of the metal foam was measured in a semi-quantitatively XRF analysis. A Philips X-ray spectrometer, type PW1480 with Uniquant 3 software was used. The measurement and its repeat were performed relative to a Teflon matrix. The XRF-sample was debris consisting of cell walls and cell edges of the metal foam that were compressed into a tablet. These cell walls and cell edges broke off during cutting of the sample. Information about the used spectrometer is compiled in the appendix 1.

The composition of the sample is mainly aluminum with additions of Ca and Ti. The material also contains a small amount of Si and Fe as pollutants, see table 5. The Ca and Ti are added in the production process of the foam, as CaO and TiH₂. The levels found deviate from the specifications, this is possibly due to an inhomogeneous distribution. When Ca and Ti are excluded, the composition of the metal is 99.57wt% Al, 0.19wt% Si and 0.118wt% Fe. This composition is consistent with a 1050 aluminum alloy, which is a technical pure aluminum, see appendix 2.

Table 5: XRF-Results of the analyzed Alporas

Element	Wt%	Std Error Wt%
Al	95.67	0.10
Si	0.182	0.010
Ca	2.66	0.08
Ti	1.26	0.06
Fe	0.113	0.006
Other elements	Each < 0.05, Total < 0.16	

4.1.2 Cell size

To characterize the structure of 9% Alporas foam, the distribution of cell sizes is determined. Photos of the structure are taken using a digital camera. Contours of the 5 times enlarged structure are copied on transparent sheet. These contours are measured using the Leica Quantymet image analysis system, which works in combination with the QWin Pro version 2.0 software.

The size of the cells in the Alporas foam was determined. The distribution of the cell size is given in figure 8 as determined with the image analyzer.

This cell diameter distribution is very similar to the cell diameter distribution of modified Alporas [37].

Separately using quantitative stereology the volume fraction and the surface area in unit volume [38] were respectively determined to be $V_v = 0.9048$ and $S_v = 1281.6$ count/m. This results in a linear intercept of 2.8 mm and a sphere diameter of 3.8 mm. In a sample cross section the number of times a specific cell size will be detected, will decrease when the size approaches the actual cell size. The reason for this is, that there is only a small chance that the cross section of a cell will result in the maximum area. This result of the quantitative stereology therefore matches with the found cell distribution.

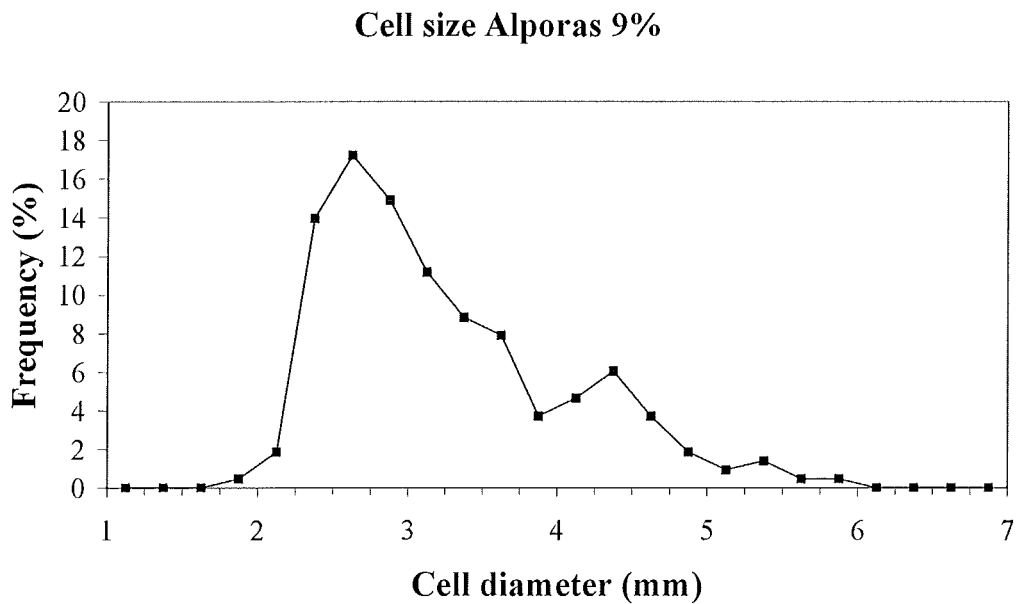


Figure 8 Distribution of cell cross sections

4.1.3 Density

The density of the material is determined from the net volume and the weight of 36 Middle Tension samples or M(T)-samples, see paragraph 4.2.1 and figure 13. The relative density is calculated against a density of 2700 kg/m^3 for solid aluminum. The foam of the samples has a relative density of 8.8%. The distribution of the relative density has a median of 8.7%, the standard deviation is 0.72%.

4.1.4 Tensile strength and hardening exponent of Alporas foam

To characterize the Alporas aluminum foam a tensile test was performed. The data from this test was used to determine the hardening exponent of the Alporas foam. The tensile strength of the Alporas aluminum foam is determined using metal foam samples. These samples have a thickness of 40 mm and the width of the gage section is 40 mm. Due to the limitations in the dimensions of the material a gage length of 190 mm is used, instead of the 200 mm recommended by the ASTM E 8-00b [39]. The layout of the used tensile test sample is shown in figure 9. The tensile test samples are made from unused samples for the FCG experiments.

The tensile test samples are mounted in the tensile test machine using the same grips as are used in the fatigue experiments. A series of five experiments resulted in a yield tensile stress of $\sigma_Y = 1.4 \text{ MPa}$ $\sigma_{n-1} = 0.2 \text{ MPa}$. The 0.2 percent offset yield strength is $\sigma_{YS 0.2} = 0.8 \text{ MPa}$. A typical tensile test curve is shown in figure 10. The experiments were performed with a stress buildup rate of 0.5 MPa/s . These experiments were performed on a *Zwick Z010 type BTC-FR010TR-A50 serial number 149933/2001*.

Although a different type of sample was used, the hardening exponent is determined from the tensile curve following the procedure of ASTM E 646-00 [40].

The hardening exponent of Alporas foam is $n = 0.47$ $\sigma_{n-1} = 0.02$.

Tensile test sample: 'Alporas aluminum Foam'

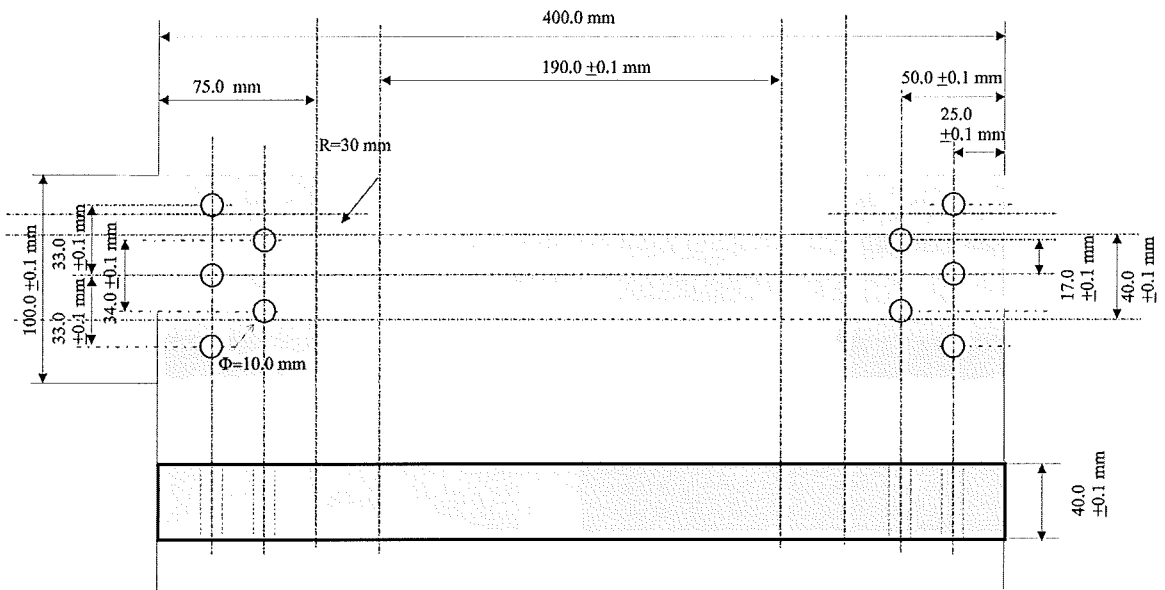


Figure 9 Aluminum foam, tensile test specimen

Tensile test Alporas Foam

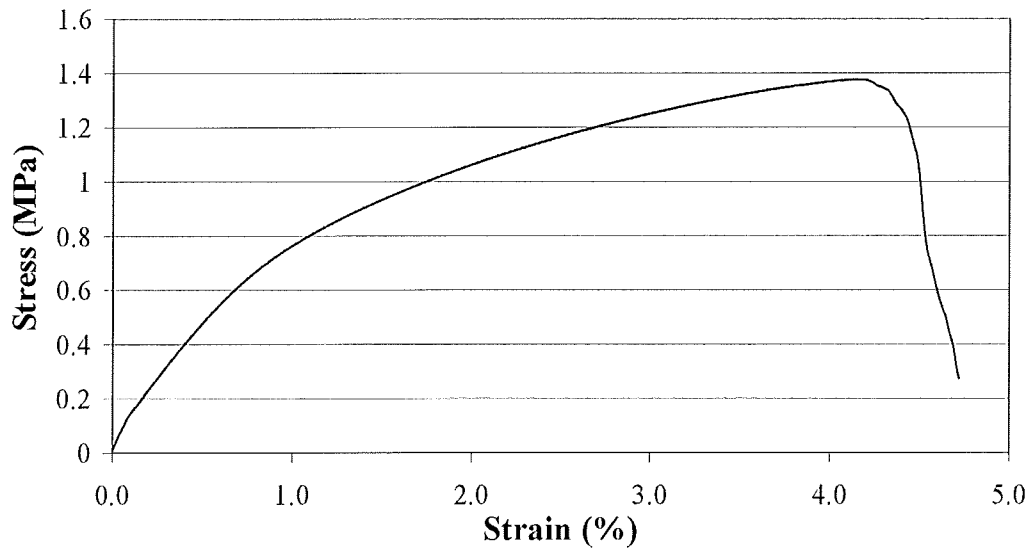


Figure 10 Tensile test Alporas aluminum foam

4.1.5 Hardness and grain size

The hardness of the material from which the foam is made is measured on a cell edge cross section, using a micro Vickers Hardness measurement. The measurements are performed with a load of $5p$ which is equal to a force of $49.03mN$.

A series of ten measurements was taken at cell edges and cell walls of a cut and polished cross section. A hardness of $HV= 32.2$ was determined, with a standard deviation of 5.3 . The same sample was etched and photographed to give an indication of the grain size, see figure 11. In figure 12 low melting phases and finely dispersed particles are visible.

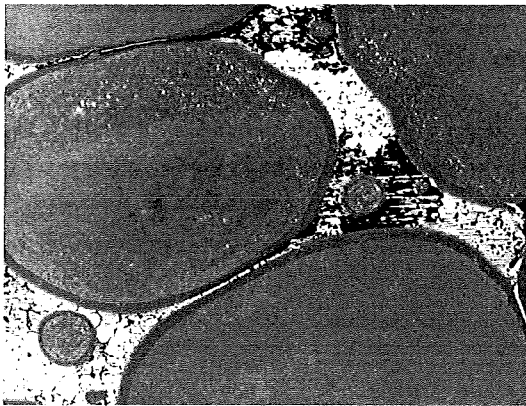


Figure 11 Grain size in the cell structure of the foam.

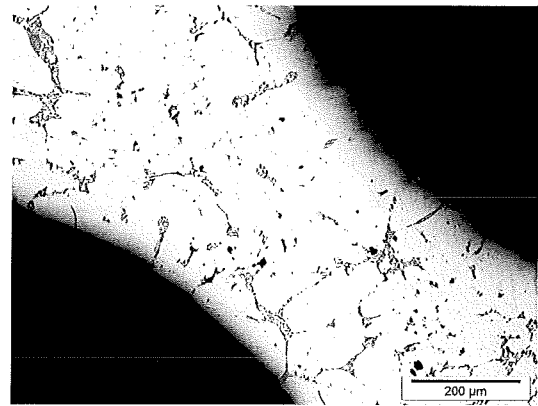


Figure 12 Low melting phases in a cell edge.

4.1.6 Hardening exponent and tensile strength of AA1050

A standard test for strain hardening is performed on annealed solid AA1050. This is done to study the behavior of the material from which the foam has been made, in a condition which approaches the solidification structure of the foam material.

The hardening exponent of an annealed aluminum alloy 1050 is determined. Prior to the experiments, the aluminum alloy 1050 was annealed for 3 hours at a temperature of $618K$.

The micro Vickers Hardness before annealing was $HV= 46.6$ $\sigma_{n-1}=1.8$ and after annealing $HV= 24.5$ $\sigma_{n-1}=1.3$. A series of ten hardness measurements was taken at a load of $100 mN$.

The tests were performed in according to ASTM E 646-00 [40]. The test sample [40] has a gage length of $60 mm$, a gage width of $12.65 mm$ and a thickness of $2.1 mm$. The experiments were performed with a stress buildup rate of $5 MPa/s$.

The hardening exponent at room temperature is 0.44 and a standard deviation of 0.06 . This result matches the results of Van Haaften for annealed AA1050 [35].

4.2 Fatigue Crack Growth testing

In this work FCG experiments are performed on a commercial available closed cell aluminum foam to investigate the Paris exponent and crack closure. The FCG experiments are performed on a center cracked specimen. The crack growth is determined by measuring the crack length as a function of the number of load cycles. This method for measuring FCG in metal foam is based on the FCG experiments in metal, as is described in ASTM E 647-00 [32].

In this part the metal foam sample, the instrumentation and the used methods are discussed.

4.2.1 Sample geometry

In the FCG test a center cracked sample is used. This center cracked sample is also known as Middle Tension sample or M(T) sample. The sample layout is shown in figure 13. The advantage of this type of sample is that it can be loaded both with positive and negative force ratios (R). Another consideration is that the FCG is not susceptible to the surface condition of the sample.

For solid metals it is common practice to cut these samples by means of wire electro discharge machining. This makes it necessary to immerse the material in a dielectric fluid. Since Alporas is porous due to structural defects, the dielectric fluid can penetrate deeply into the material and can possibly influence the fatigue process. For this reason mechanical machining of the sample is preferred.

The apparent strength of foam test samples depend on the ratio of the sample size to the cell size, and can be influenced by the state of the surface and the way in which the sample is gripped and loaded. In work done by Onck [41] it was found that the sample size has influence on tensile tests. For this reason a standard sample thickness T of 40 mm was chosen instead of the recommended range by ASTM E 647-00 [32] ($W/4 \geq B \geq W/8$). In this way the sample has more than seven cell diameters in the thickness direction [6 and 7]. The total sample configuration is $400 * 100 * 40$ mm ($H * W * T$). The 400 mm dimension of the sample is the same as the 400 mm dimension of the delivered plates.

Due to internal defects in the material it is necessary to use an initial crack of $a_n \geq 13$ mm, instead of the $2a_n \geq 0.2 * W$ centered notch recommended by the ASTM E 647-00.

The ΔK or Feddersen formula for a M(T) sample is:
$$\Delta K = \frac{\Delta P}{W * B} \sqrt{\frac{a\pi}{\cos \frac{a\pi}{W}}} \quad (8)$$

In this equation a is the crack length, W is the sample width, B is the sample thickness, ΔP is load range ($\Delta P = P_{max} - P_{min}$) and ΔK is the range of the stress intensity factor.

ASTM E 647-00 [32] requires the sample to be predominantly elastic at all values of the applied force. In case of a M(T) sample the following is required:

$$(W - 2a) \geq 1.25 P_{max} / (B \sigma_{ys}) \quad (9)$$

Where P_{max} is the maximum load and σ_y is the yield stress. The other parameters are the same as before.

To determine the influence of the sample thickness, M(T) samples are used with a thickness of 40, 35, 30, and 20 mm. These samples are made from the M(T) samples which are used in this work.

M(T) sample: 'Alporas aluminum Foam'

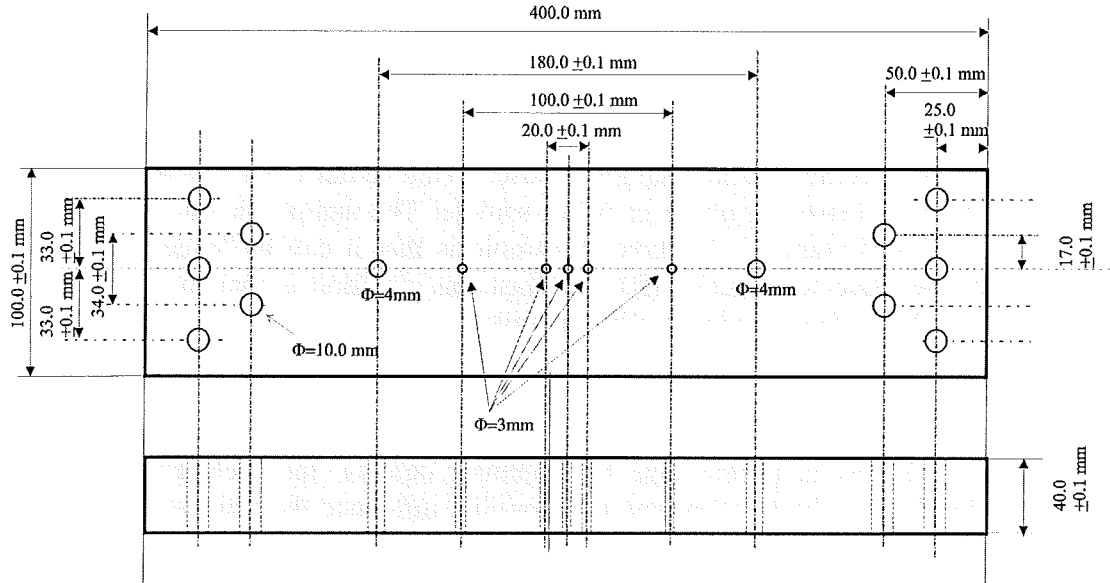


Figure 13 Layout of used M(T) sample.

4.2.2 Instrumental setup

The FCG experiments are performed by cyclic loading of a sample and measuring the crack length as a function of the number of load cycles. In this part the methods and instrumentation for cyclic loading and measuring the crack length is discussed.

4.2.2.1 Fatigue testing apparatus

The fatigue experiments were performed using a Schenck Hydropuls PSB with a load-cell of $100kN$, see figure 14. The error in the load measurement is $30N$. The experiments to determine the influence of the sample thickness were performed on a different machine of the same model but equipped with load-cells of $2kN$ and $10kN$. The $10kN$ load-cell has an error of $4N$.

The M(T) sample was mounted in the grips by using friction plates. The friction plates are used at the front and back to clamp the sample, see figure 15. This was done at the bottom and at the top of the sample. Each set of friction plates was clamped with five bolts. The friction plates fit tightly in holders. Crushing of the foam is avoided.

The grips are electrically isolated from the test frame to avoid interference with the crack length measurement. The electrical resistance of the grip isolation is greater than $19M\Omega$.

A nut and bolt connection is used for the electrical connections at the sample. An $M3$ size is used for the potential drop measurement and $M4$ size for the current connection.

The bolts were tightened by hand and extra rings were used to avoid crushing the foam. The used rings have an outer diameter of 12 mm , for the potential drop measurement and 25 mm for the lead connections.

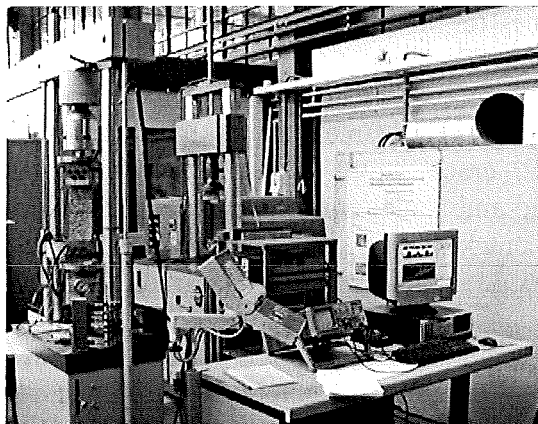


Figure 14 Overview Schenck Hydropuls PSB

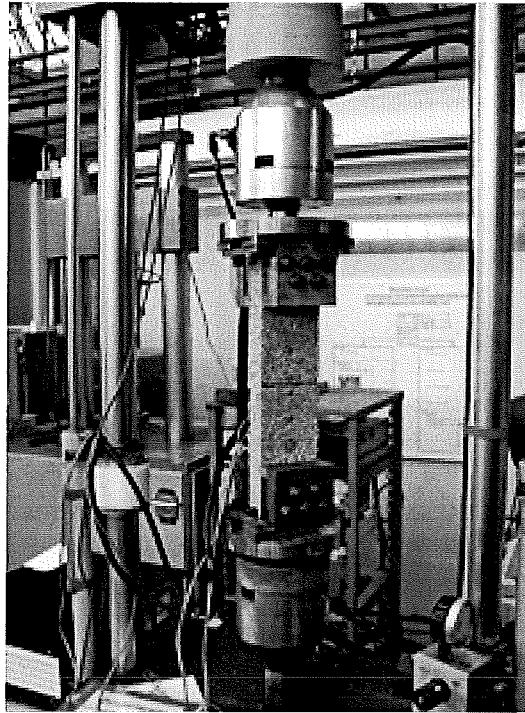


Figure 15 Position of the sample in the fatigue testing apparatus

4.2.2.2 Measurement of Fatigue Crack Growth

The pulsed DC potential drop method is used to measure the crack length in metal foam. This method is used in solid metals for the same purpose.

In this method a pulsed electrical current is passed through the sample, while the potential drop due to a crack is measured, see figure 16. The pulsed current is only on during the potential drop measurement. This is to prevent the heating up of the sample [42]. The pulsed DC current is synchronized with the fatigue load cycle. The potential drop is measured at the maximum load during the cycle, when the crack has its widest opening. All influences on the potential drop measurement, except the crack length, are eliminated by using the ratio of two potential drops over the crack, measured at two different distances to the crack. The ratio of the measured potential drops is a measure for the crack length. Crack length measurements are performed using a Howden pulsed D.C. crack length measuring system. The empirical correlation between the measured and actual crack size is determined in a calibration test and is used to calculate the crack length, see paragraph 4.2.2.3. The settings of the Howden are shown in appendix 3.

The measured signal is amplified and stored in a computer at chosen time intervals. During the experimental program the computer was updated to perform the following tasks:

- Conversion of the potential drop to crack length.
- Periodical storing the process parameters as measured force, crack length and cycle number.
- Compile programmable processes.
- External process control of the Schenck Hydropuls PSB.

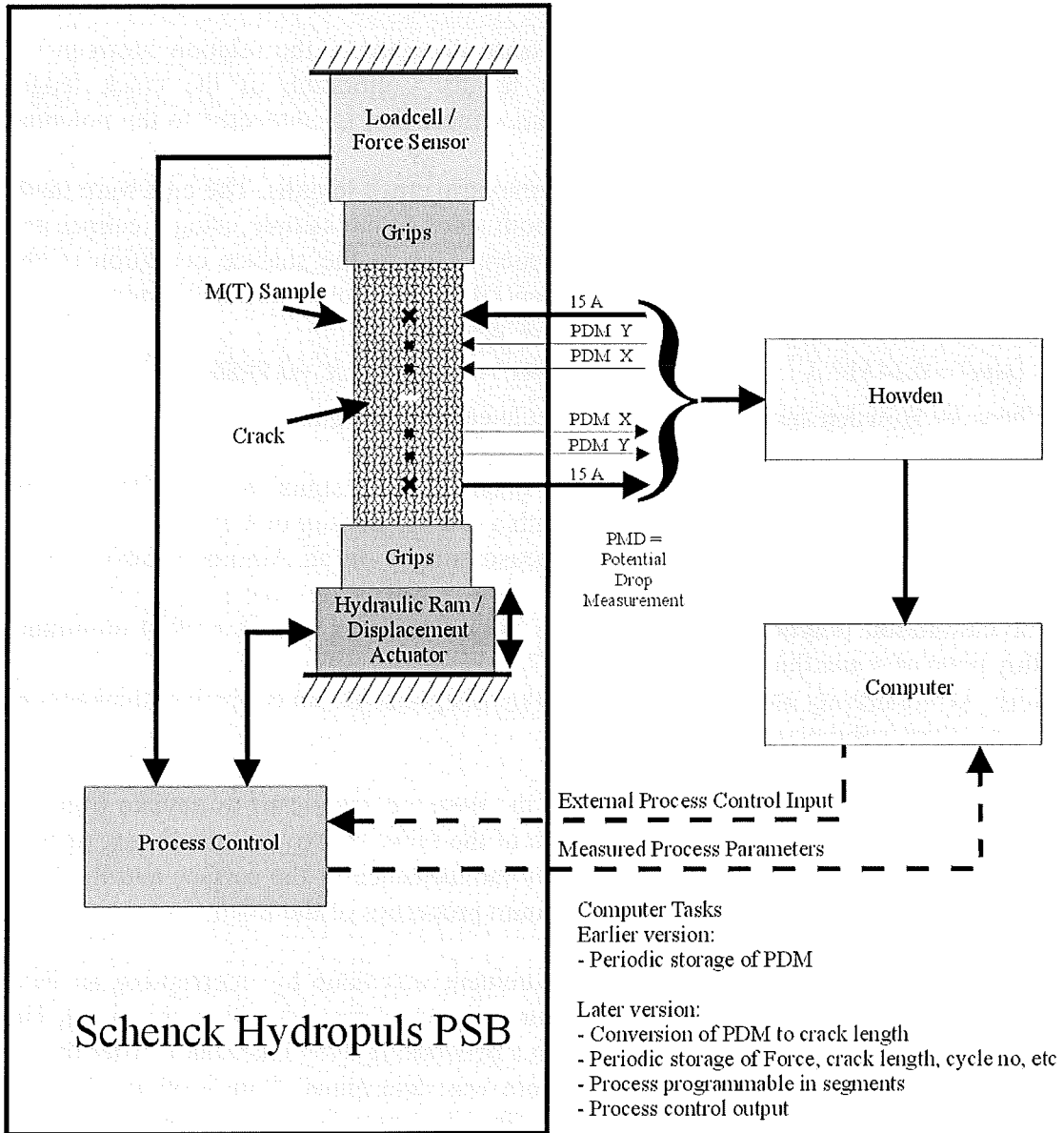


Figure 16 Experimental setup

4.2.2.3 Calibration crack length measurement

Prior to the FCG experiments it is necessary to calibrate the relation between the measured potential drop and the crack length. Calibration of the crack length measurement is performed on a metal foam sample that is connected to the potential drop measurement.

The signal is measured for a number of symmetric crack lengths. The cuts were made with a saw. The saw cut is measured on both sides of the sample using a caliper and checked with the potential drop measurement. Due to the surface condition of the aluminum foam the error in the measurement of the saw cut is 0.25 to 0.5 mm.

The data is used to fit a 3rd order polynomial equation;

$$a \text{ (mm)} = 0.1451 * X^3 - 1.9699 * X^2 + 16.341 * X - 24.22, R^2=0.9996$$

Where X = Howden signal and a is the calculated crack length.

This function for the conversion of the potential drop signal to crack length was determined on an Alporas M(T) sample with a relative density of 8.1%.

This result was reproduced by similar measurements on an Alporas sample with a density of 10.9%, see figure 17.

The calibration polynomial of Alporas is very similar to that of a 2024 aluminum alloy plate of 4 mm thickness, see figure 17.

Note. At 9% density and a thickness of 40 mm Alporas has an equivalent thickness of 3.6 mm thick solid plate.

At a crack length of 40 mm ($2a=80$ mm) the measurements start to deviate from the fit. At this point the remaining ligament is in the order of two cell diameters, at both ends of the sample. In these circumstances the influence of the surface and the local cell properties will prevail over the continuum properties of the foam.

Another check of the crack length measurement was done by interrupting an FCG experiment before failure and by determining the actual crack length at this point. The fatigue crack of the sample is sprayed with a penetrating dye (Traceelac). After drying the sample was strained and the crack front was determined from a photo. A crack length of $a= 22.3$ mm versus 22.71 mm for the potential drop measurement was found.

The crack front in the sample was found to vary in length over the thickness of the sample.

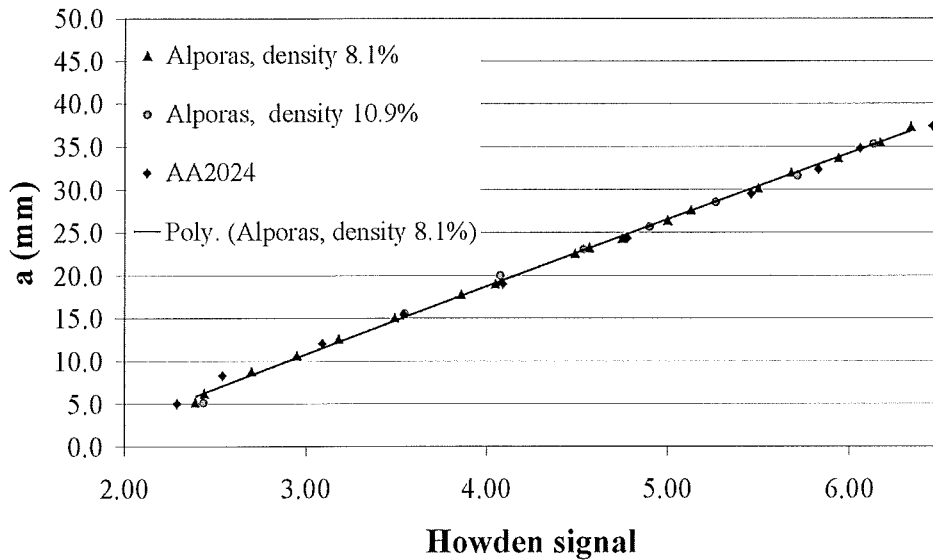


Figure 17 Howden calibration curve

4.2.3 Practices for FCG experiments

The following practices are observed in the FCG experiments.

At the start of a FCG experiment an initial crack is made by a saw cut, in the middle of the M(T)-sample width. This saw cut is approximately 0.8 mm wide and the $2a$ length is $\geq 26\text{ mm}$ ($a \geq 13\text{ mm}$). Due to the present internal defects in the form of big cells, it is necessary to have an initial crack length of at least 13 mm . These big cells were formed during the production process by coalescence of cells.

The saw cut is measured on both sides of the sample using a caliper and checked with the potential drop measurement. If necessary the conversion equation will be adjusted in the least significant constant.

The FCG experiments are performed with an increasing stress intensity (ΔK) regime, either with a constant load amplitude or with a gradually increasing load. Note. This procedure is applicable for crack growth rates of 10^{-8} m/cycle and higher [32].

Experiments are performed with a sinus load at a frequency of 5Hz. Note. The present system is not capable of controlling a gradually decreasing load.

Prior to the measurements the sample is pre-cracked. During pre-cracking the initial crack length will increase 4 mm at each crack front. Pre-crack is performed either with constant ΔK or with constant load amplitude.

The σ_{\max} of the load is chosen in the range of 25 to 33% of σ_y . During the experiment load changes are limited to 20% at a time. Between load changes there must be a noticeable crack growth. FCG experiments are conducted for load ratios of $R=-1, -0.5, -0.25, 0.1, 0.5$ and 0.7 .

Experiments to determine the influence of the sample thickness are conducted at a load ratio of $R=0.1$.

4.2.4 Data analysis

The measured data from the FCG experiments is put into an input file for the program *Visual Fatigue*. This input file is a Comma Separated Value or CSV file and contains columns with the number of cycles, the crack length, the maximum load and the minimum load in *kN*. The program visual fatigue makes an interpolation of the raw data and calculates the ΔK using the Feddersen formula (8). Other input criteria are the sample thickness in millimeters and the step in the crack length of 0.05 mm.

In solid metals only the tensile or positive part of a fatigue load plays a part in the crack growth. Therefore ASTM E 647-00 [32] prescribes the use of $\Delta P = P_{max}$ at load ratios of $R \leq 0$.

In foams both a compression load and a tensile load deform the material in bending, see figure 2. For this reason $\Delta P = P_{max} - P_{min}$ is used instead. In the program *Visual Fatigue* the ΔK is based on $\Delta P = P_{max} - P_{min}$.

To visualize the Paris region of the FCG curve the data is plotted on a double log scale.

4.3 SEM

To complement the FCG experiments the failure behavior of the metal foam is studied by investigating the fracture surfaces with a Scanning Electron Microscope (SEM). These samples were tested with load ratios of $R=-1$ and $R=0.5$. The samples were cleaned in an ultrasonic bath of iso-propanol before they were placed in the SEM.

The fracture surface is investigated with a Jeol JSM-6500F field Emission Scanning Electron Microscope. This SEM has a Schottky type field emission (T-Fe) gun with a Zr/O tungsten emitter, for a narrow beam. An acceleration voltage of 15 keV was used. Local composition of the fracture surface can be measured using Energy Dispersive Spectroscopy (EDS).

The range of the electrons in the material dictates the volume from which the composition is measured. At 15 keV the range in aluminum is $2.2\ \mu\text{m}$ [43].

5 Results

In this part the results of the FCG experiments and the fracture surfaces are presented. First the general shape and position of the curves is shown in paragraph 5.1. In paragraph 5.2 the Paris exponent m of the FCG curves is presented. In paragraph 5.3 two crack closure fits are presented. These fits are made for two different assumed influences of the applied ΔK on the FCG. In paragraph 5.4 the results of the fracture surface investigation are presented.

5.1 Fatigue Crack Growth curve of Alporas aluminum foam

As an example two measured FCG curve are shown in figure 18. The FCG is similar to region II and III in figure 3. The curve seems to differ from a typical FCG curve in the region of crack initiation.

Other deviations compared with solid aluminum are the bumpiness of the measured curves and the variation in the location of the curve. During the FCG experiments it is not possible to follow the crack growth visually on the sample surface.

The results of the FCG measurements for R -values of -1 , -0.5 , -0.25 , 0.1 , 0.5 and 0.7 are displayed in figure 19. Only successful experiments are displayed.

Practical limitations on the experiment duration and the low yield strength of the material made it very difficult to perform an experiment at a load ratio of $R=0.7$. The FCG experiments with positive R -values do not meet the ASTM requirement [32] for the sample to be predominantly elastic, see paragraph 4.2.1. To avoid extreme long duration experiments it was decided to use these experiment results.

The FCG curves have a relatively big spread. The spread is taken as the range in stress intensity that includes the measured FCG curves, at the crack grow rate of $da/dN= 10^{-2} \mu\text{m}/\text{cycle}$. Five measured FCG curves with a load ratio of $R=0.1$ have an average value ΔK of $0.0110 \text{ MPa}\sqrt{\text{m}}$ ($\sigma_{n-1}=0.0079 \text{ MPa}\sqrt{\text{m}}$) at a value of $da/dN= 10^{-2} \mu\text{m}/\text{cycle}$. The spread in ΔK for these curves is $0.022 \text{ MPa}\sqrt{\text{m}}$ at $da/dN= 10^{-2} \mu\text{m}/\text{cycle}$. The values of K_c were determined for a crack grow rate of $da/dN= 10^{-2} \mu\text{m}/\text{cycle}$, from extrapolated FCG curves. These approximated K_c values range from 0.142 to $0.249 \text{ MPa}\sqrt{\text{m}}$.

Of the experiments performed with the load-cell of 10kN , two FCG curves of M(T)-samples with a thickness of 30 mm and $R=0.1$ have a spread in ΔK of $0.0088 \text{ MPa}\sqrt{\text{m}}$ at $da/dN= 10^{-2} \mu\text{m}/\text{cycle}$.

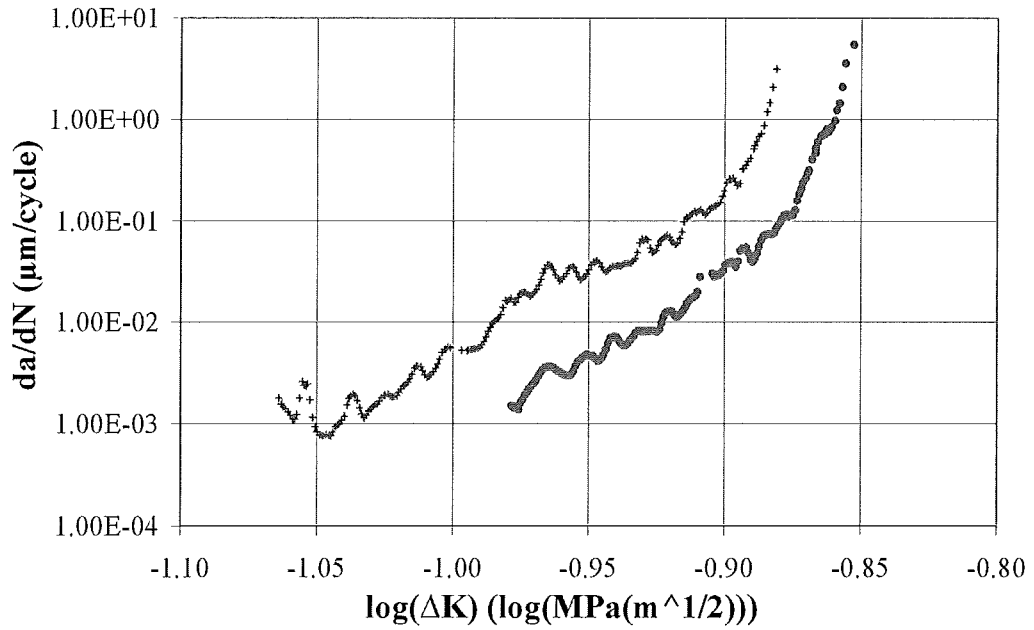


Figure 18 Example of measured Alporas aluminum foam FCG curve at R=0.1

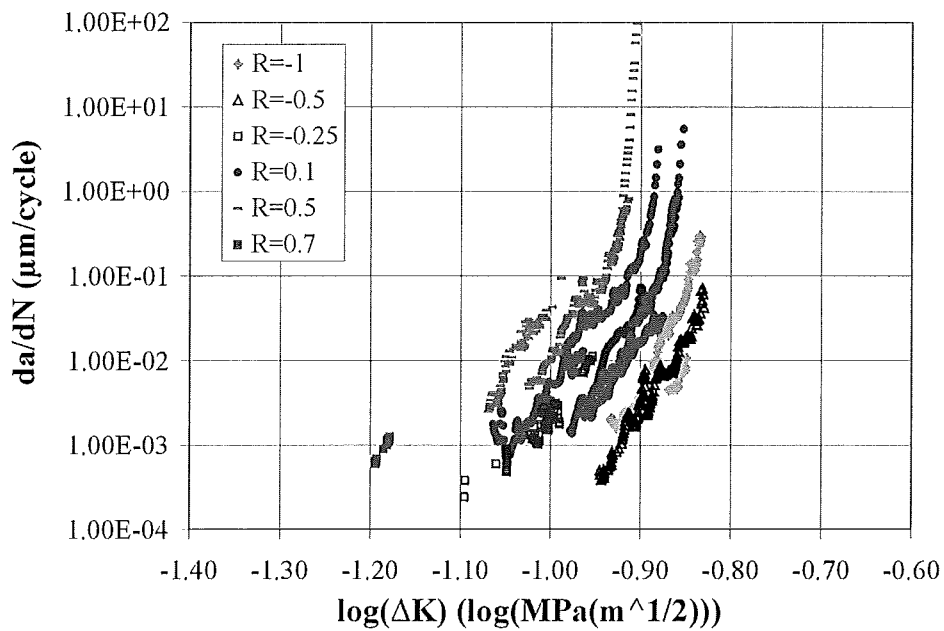


Figure 19 Measured Alporas aluminum foam FCG data, R values of -1, -0.5, -0.25, 0.1, 0.5 and 0.7

5.2 Paris exponent

The Paris exponent m is determined from the more or less linear part of the measured FCG curve, that is assumed to be the stable crack growth stage. This is done by fitting a linear function on the bi-logarithmic representation of the stable crack growth stage of the FCG curve. The Paris exponent m is determined for the ten curves shown in figure 19. The median of these exponents is 15.6 with a standard deviation of 1.5, see figure 20 and table 6. Note. The FCG curve with load ratio $R=0.7$ extremely short, which made it hard to determine the Paris exponent. However this value could not be excluded on a statistical argument.

The experiments with thinner samples were performed on a different Schenck Hydropuls PSB testing machine, equipped with load-cells of 2 kN and 10 kN . Two experiments with a sample thickness of 40 mm were performed with the 10 kN load-cell, to enable a comparison between the experiment sets of both machines.

The FCG experiments with thinner M(T)-samples show an increase in the Paris exponent for a sample thickness smaller than 35 mm .

Note. The M(T)-sample was scaled to have 8 cell diameters, to avoid influence of the surface [41] and to reduce the influence of an inhomogeneous cell structure. This was based on the literature value for the cell diameter of 4.7 mm .

An overview of the performed FCG experiments is given in table 6.

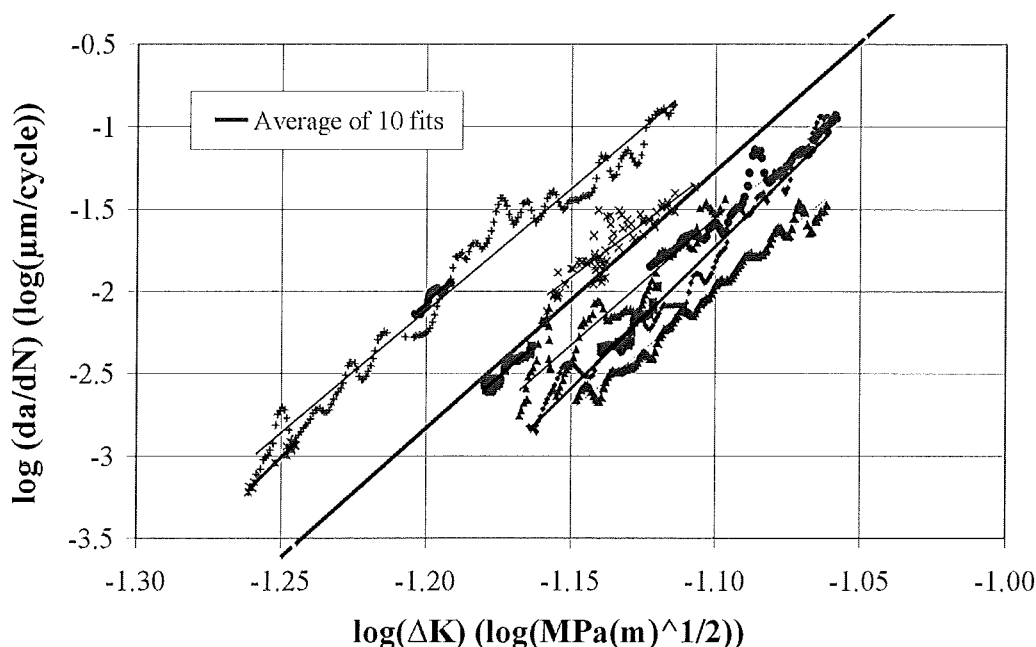


Figure 20 Fitted Paris exponents

Table 6: Experimental Paris exponents.

Paris exponents, determined from FCG experiments			
Sample Thickness (mm)	Load ratio R	Load cell used (kN)	Paris exponent <i>m</i>
40	-1	100	16.7
40	-1	100	15.5
40	-0.5	100	15.6
40	-0.25	100	17.0
40	0.1	100	17.4
40	0.1	100	14.0
40	0.1	100	14.6
40	0.1	100	14.9
40	0.5	100	13.2
40	0.7	100	17.8
40	0.1	10	16.6
40	0.1	10	18.0
35	0.1	10	14.9
30	0.1	10	16.1
30	0.1	10	21.2
20	0.1	10	21.9
20	0.1	10	19.0
20	0.1	2	19.5

5.3 Crack closure

A crack closure effect causes a shift in ΔK of a FCG curve. This shift is dependent on the load ratio of the measured curve and is relative to the position of the FCG curve measured at a load ratio of $R=1$, where closure is assumed to be absent.

From the location of the FCG curves in figure 19, it is clear that the crack closure phenomenon is present, due to the shift in position in relation to the load ratio.

In literature and ASTM [32] it is assumed that the compression part of the load doesn't contribute to the FCG. However, in this work a contribution of the compression part of the load to the FCG is expected, see paragraph 2.3.

To solve these conflicting views, a comparison is made between two crack closure fits. The first crack closure fit is made using the total available ΔK . This fit is designated *Foam ΔK approach*. The second crack closure fit is made using the positive part of the available ΔK , thus excluding the compression part of the load. This fit is designated *ΔK approach according to ASTM*.

To determine the effect the crack closure has on the position of the FCG curve, the shift is fitted with respect to the load ratio. Both fits are made with the 10 FCG curves shown in figure 19. The following restriction was imposed on the coefficients of the fitted function ($a+bR+cR^2$), $a+b+c=1$. Ideally a crack closure fit would move all the curves to the location of the FCG curve with load ratio $R=1$.

5.3.1 Foam ΔK approach

The crack closure fit for *Foam ΔK approach* is made using $\Delta P=P_{max}-P_{min}$ for load ratios $-1 \leq R \leq 1$. The optimized polynomial function $U=0.63+0.23R+0.14R^2$ is fitted to obtain the effective ΔK of each curve. The fitted crack closure functions U for *Foam ΔK approach*, *ΔK approach according to ASTM* and the Schijve function [31] are shown in figure 22.

In the *Foam ΔK approach* fit the spread in ΔK at $da/dN=10^{-2}$ $\mu\text{m}/\text{cycle}$ is reduced from $\Delta K=0.052$ $\text{MPa}\sqrt{\text{m}}$ to 30% or $\Delta K=0.0153$ $\text{MPa}\sqrt{\text{m}}$. This spread is comparable to the spread in the five measured curves at $R=0.1$. The spread in the da/dN bandwidth is reduced from a max/min ratio of 460 to 44, compare figures 19 and 21.

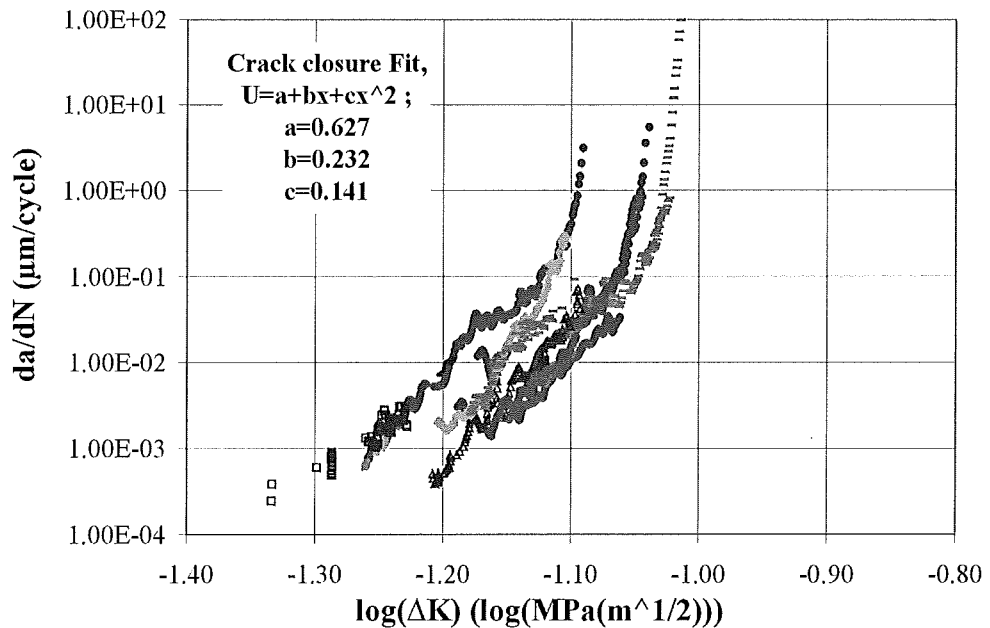


Figure 21 Result of crack closure fit.

5.3.2 ΔK approach according to ASTM

The crack closure fit for the ΔK approach according to ASTM is made using only the positive part of the load. For load ratios $R < 0$ $\Delta P = P_{max}$ is taken into account. For load ratios $0 \leq R$ $\Delta P = P_{max} - P_{min}$ is taken into account.

The optimized polynomial function $U = 0.576 + 0.015R + 0.409R^2$ is fitted to obtain the effective ΔK . The resulting reduction in ΔK spread is very similar to the case where the Foam ΔK approach is taken. The spread in ΔK of results is $\Delta K = 0.0176 \text{ MPa}\sqrt{\text{m}}$ at $da/dN = 10^{-2} \text{ }\mu\text{m/cycle}$.

The fitted curve in the ΔK approach according to ASTM is a parabola where the effective fraction of the positive ΔK has a minimum at $R = 0$ and the greatest fraction at $R = 1$ and $R = -1$.

The fitted crack closure functions U for Foam ΔK approach, ΔK approach according to ASTM and the Schijve function [31] are shown in figure 22.

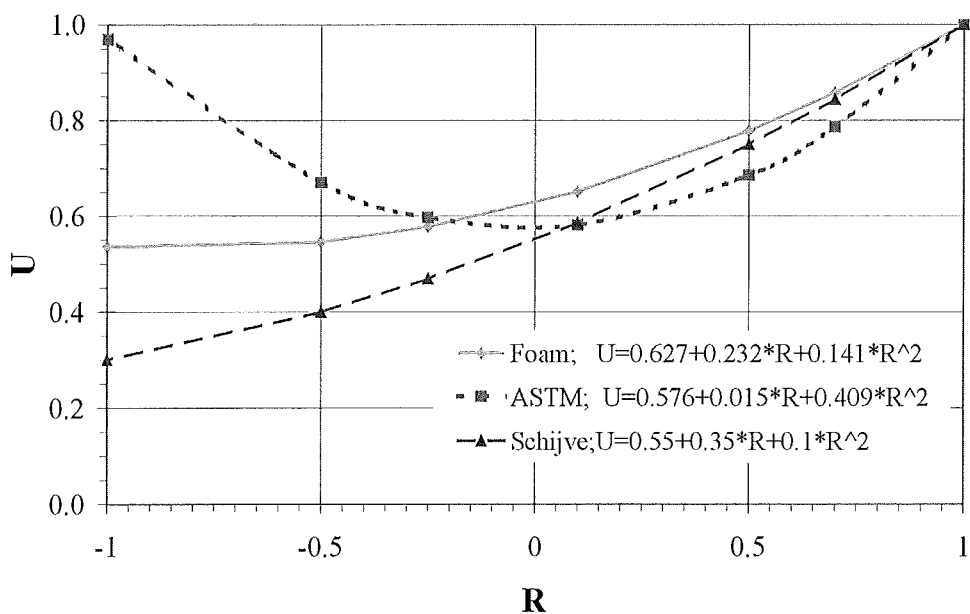


Figure 22 Fitted curves $U=f(R)$

5.4 Fracture surfaces

The fracture surfaces of two FCG samples were investigated with a SEM, to learn more of the failure behavior of the metal foam. Those samples were subjected to load ratios of $R=-1$ and $R=0.5$ during the FCG experiments.

The fracture surfaces are a mixture of ductile behavior, plastic deformation, slant fracture (figure 23), dimples and tearing (figure 24). The surface is rough, it contains particles, cracks and defects, see figures 23, 24, 25, 26, 27 and 28. In the sample with load ratio $R=0.5$ there is a definite occurrence of slip.

The composition of the material is mainly a fairly pure aluminum with areas where Ti, Ca, Fe and O is present. Also there are inclusions of Ti and Ca rich particles, see figures 29, 30 and 31.

In the places with the best-defined striations oxygen is found together with Ti+Ca or Ca or Fe, see figures 32, 33, and 34.

Note. The EDS spectrum taken at these places is diluted by the signal of underlying material.

Striations are less well defined and clearly influenced by plasticity at places with oxygen and aluminum, see figures 27, 29 and 30. The striations in figure 33 have a spacing of about $0.1 \mu\text{m}/\text{cycle}$, possibly they were created at the start of the fatigue process.

When only aluminum is present the fracture surface has a very plastic nature, figures 23 and 30.

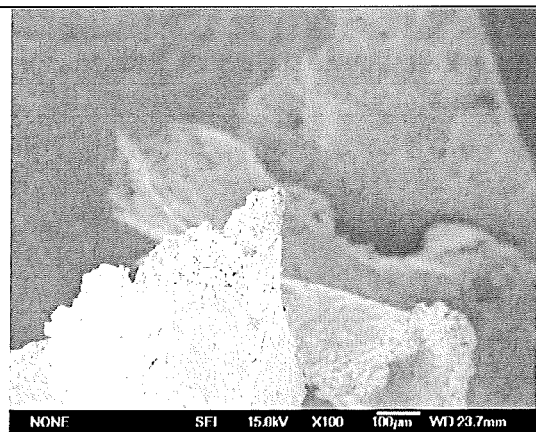


Figure 23 Failed cell edge, slant fracture. Sample $R=0.5$

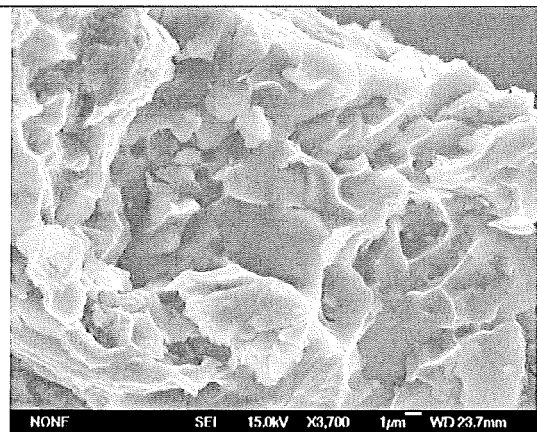


Figure 24 Plastic behavior during failure. Dimples and slip. Sample $R=0.5$

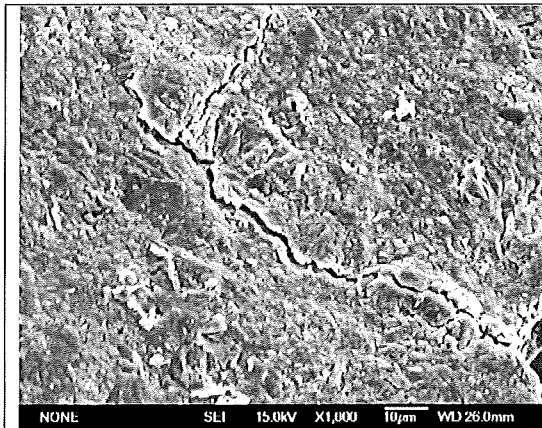


Figure 25 Crack tip, Sample R=-1.

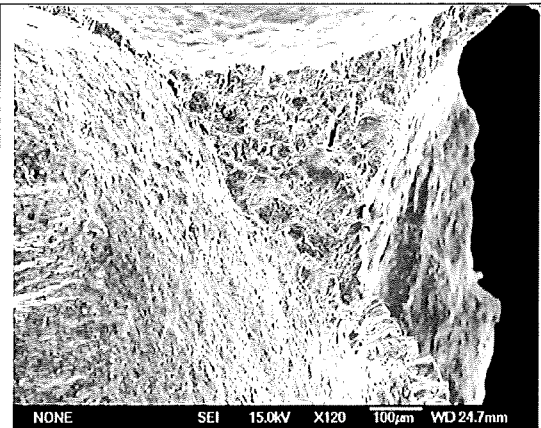


Figure 26 Failed cell edge, top view.
Sample R=-1

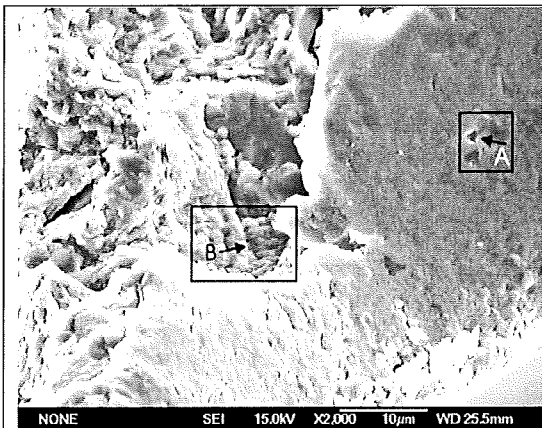


Figure 27 Sample R=-1. A Defect in surface of cell wall. B Striations

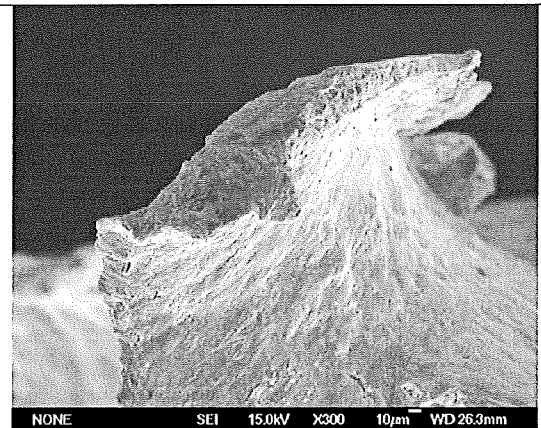


Figure 28 Fracture surface of a failed cell wall, sample R=0.5

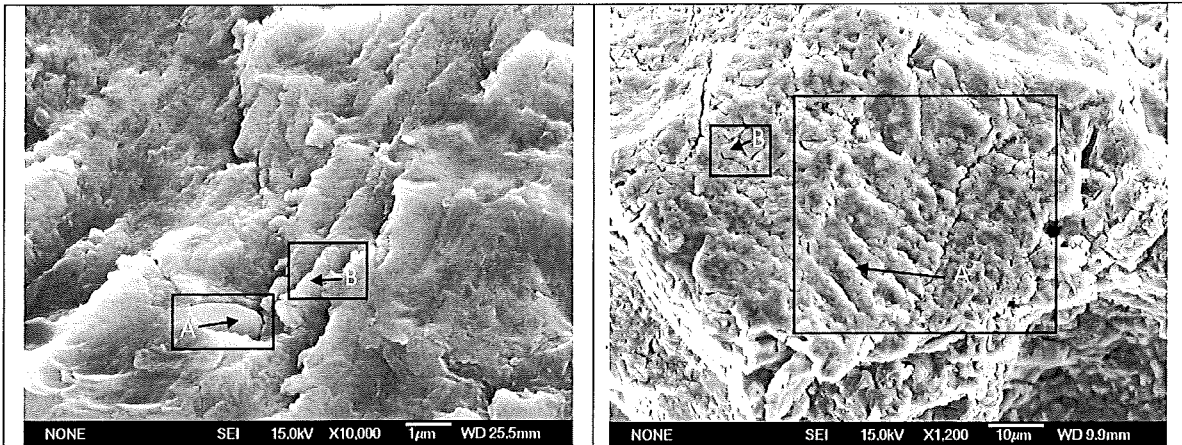
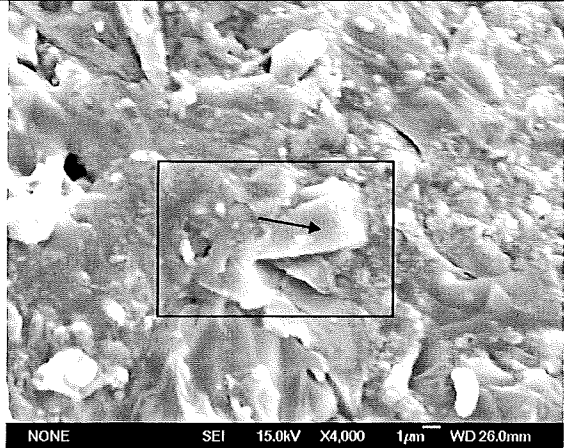
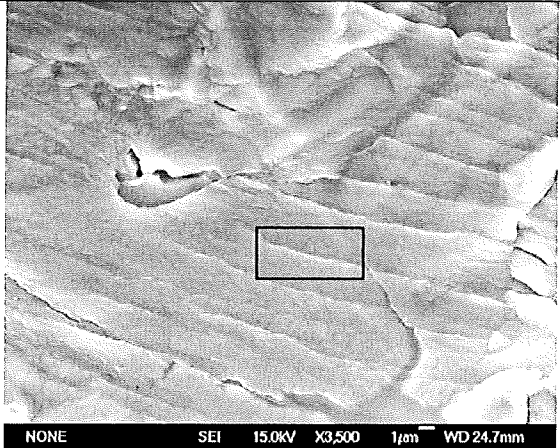


Figure 29 Ti particle and striations in oxygen rich areas. Sample R=-1

Figure 30 Striations in oxygen rich areas. Ca particle. Striation spacing 5 to 9 μ m. Sample R=-1

Element	A. Particle Wt% +/- σ_{n-1}	B. Striation Wt% +/- σ_{n-1}	Element	A. Striation Wt% +/- σ_{n-1}	B. Particle Wt% +/- σ_{n-1}
Al	80.12 +/- 0.19	86.32 +/- 0.19	Al	85.84 +/- 0.19	72.60 +/- 0.17
O	12.51 +/- 0.65	13.52 +/- 0.54	O	13.86 +/- 0.30	16.07 +/- 0.65
Ca	2.41 +/- 0.06	0.08 +/- 0.02	Ca	0.20 +/- 0.02	11.29 +/- 0.09
Ti	4.90 +/- 0.07	0.06 +/- 0.02	Ti	0.08 +/- 0.02	0.00 +/- 0.00
Si	0.00 +/- 0.00	0.00 +/- 0.00	Si	0.00 +/- 0.00	0.00 +/- 0.00
Fe	0.06 +/- 0.03	0.01 +/- 0.03	Fe	0.02 +/- 0.03	0.04 +/- 0.03

			
<p>Figure 31 Ca particle. Sample R=-1</p>		<p>Figure 32 Striations in Ca and O rich area. EDS measurement in the middle of striation. Striation spacing 2 to 3µm. Sample R=0.5.</p>	
Element	Particle Wt% +/- σ_{n-1}	Element	Striation Wt% +/- σ_{n-1}
Al	81.45 +/- 0.19	Al	83.83 +/- 1.02
O	1.50 +/- 0.22	O	9.53 +/- 1.07
Ca	6.67 +/- 0.14	Ca	5.95 +/- 0.72
Ti	0.00 +/- 0.02	Ti	0.23 +/- 0.35
Si	0.00 +/- 0.00	Si	0.03 +/- 0.30
Fe	0.01 +/- 0.03	Fe	0.44 +/- 0.87

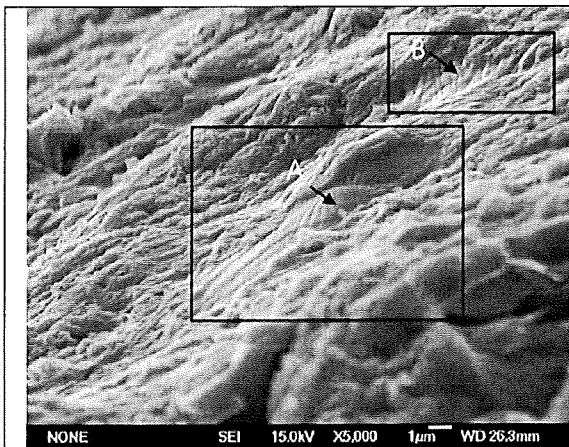


Figure 33 Striations in Fe and O rich areas. Striation spacing 0.2 to 0.4 μ m. Dimples in the lower right corner. Sample R=0.5

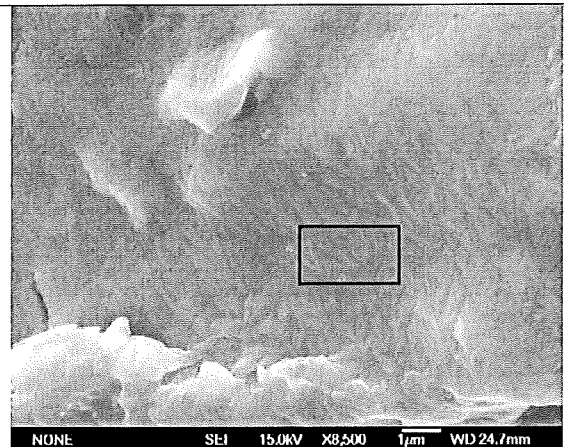


Figure 34 Striations in Ca rich areas, R=-1

Element	A. Striation Wt% +/- σ_{n-1}	B. Striation Wt% +/- σ_{n-1}	Element	A. Striation Wt% +/- σ_{n-1}
Al	76.21 +/- 8.25	68.01 +/- 9.25	Al	81.82 +/- 0.19
O	13.49 +/- 13.49	26.56 +/- 14.49	O	11.82 +/- 0.55
Ca	0.00 +/- 0.00	2.23 +/- 3.34	Ca	16.52 +/- 0.08
Ti	0.00 +/- 0.00	0.00 +/- 0.00	Ti	0.16 +/- 0.04
Si	1.71 +/- 3.42	0.00 +/- 0.00	Si	0.00 +/- 0.00
Fe	8.59 +/- 5.73	3.20 +/- 6.40	Fe	0.00 +/- 0.00

6 Discussion

6.1 Failure mode

It is clear from the fracture surfaces, that the solid material of the foam is rather heterogeneous. The composition at the fracture surface varies. Particles that were used in the foam production process are found at the foam surfaces and at the fracture surface. The material also contains defects on the surface of the cell edges and cell faces. The cell structure contains big cells that were formed during the production process by coalescence of cells.

Striations of the fatigue process are especially found in places where the composition deviates and contains oxides.

In general the fracture surfaces show a ductile failure mode, with evidence of slip and plastic deformation.

Based on the SEM photos of the fracture surfaces, it is most likely that the crack closure effect is caused by surface roughness. This roughness is a result of plastic deformation during FCG or the meandering crack growth path through the irregular cell structure.

6.2 Fatigue Crack Growth curves

In principle the FCG curves of the Alporas foam are the same as in the schematic FCG curve of figure 3. The experimental FCG curves are shown in the figures 18 and 19. The foam FCG curves deviate from the schematic curve in the region of crack initiation. This is possibly the influence of the short crack growth phenomena on the crack initiation. More work needs to be done on this subject.

The fact that the FCG curves with positive load ratio do not meet the elastic requirements (see paragraph 4.2.1) of the ASTM E 647-00 [32] is not considered to be a problem. The Paris exponents determined at these curves are in the same range as the Paris exponents of the other curves. Both elastic and plastic parts of the FCG curves can be used for the determination of the crack closure effect.

The range of the Paris region is about $0.03 \text{ MPa} \sqrt{m}$. This implies that the entire Paris region is close to the unstable crack growth region where plastic failure mode can be expected.

Figure 35 shows the contrast between two of the experimental foam FCG curves and an FCG curve of a solid aluminum alloy, AA5083 [44]. The foam curves are the same as in figure 19.

From the experimental results it is clear that crack initiation has a threshold value $\Delta K_{TH} < 0.095 \text{ MPa} \sqrt{m}$ at $R=0.1$. The critical stress intensity K_c varies approximately from 0.14 to $0.25 \text{ MPa} \sqrt{m}$ at $R=0.1$ and a crack grow rate of $da/dN = 10^2 \text{ } \mu\text{m/cycle}$.

The spread in the FCG curves with the same load ratio is partly due to the error in the load control of the fatigue test instrumentation. The increase in accuracy of the force measurement did not have a reducing effect on the spread of the FCG curves. The

results of the 10 kN load cell experiments suggest a spread in ΔK to be in the same order as the spread of the 100 kN load cell experiments. The remaining spread in ΔK is apparently due to the material, since the error in the 10 kN load cell experiments is relatively small.

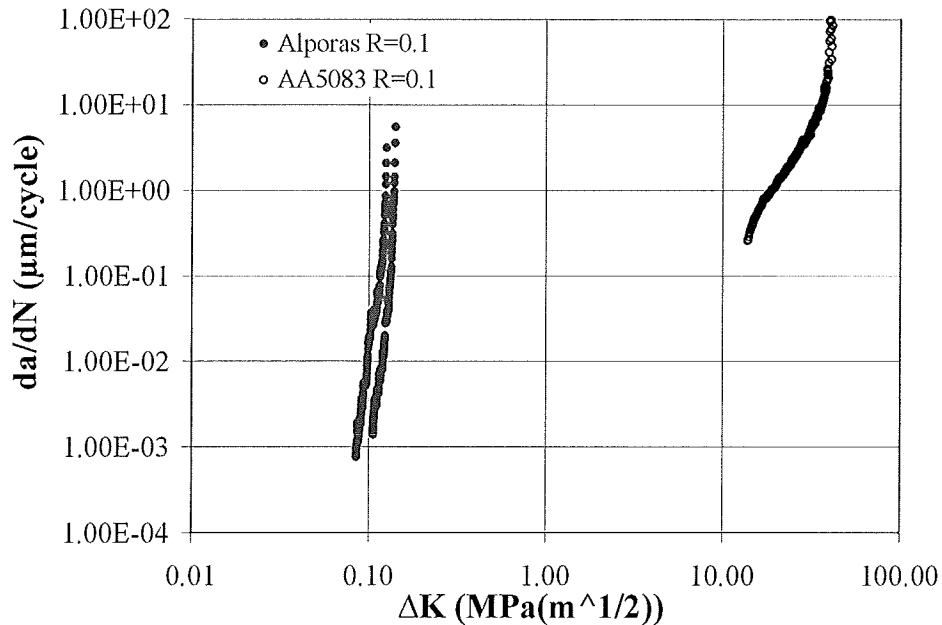


Figure 35 Comparison between FCG curves of Alporas foam and solid AA5083.

6.3 Paris coefficient; experimental and literature

The median of the determined Paris exponents is 15.6 with a standard deviation of 1.5 . The Paris exponents determined from FCG curves with positive load ratio are in the same range as the Paris exponents of the other curves.

These Paris exponents differ from the value of 25 found in the literature [15]. This deviation possibly results from factors as a different type of sample, other sample thickness and other foam density.

Experiments show that a thinner sample thickness has a boosting effect on the Paris exponent. This influence of the sample surface has been reported before by Onck [41]. The Paris exponents of samples with a thickness of 35 mm and greater are within the range of Paris exponents determined on the standard samples.

6.4 Paris coefficient and *Beam Bending* model

The experimental FCG curves of the Alporas foam are used to test the *Beam Bending* model. The plastic nature of the fracture surfaces suggests that the low cycle fatigue version of the *Beam Bending* model (formula(6)) is applicable.

In this model the following foam parameters are used:

- The cell wall length $l = 2.2 \text{ mm}$. This is approximated by calculating a cell wall length for a two dimensional hexagonal cell from the determined cell diameter of 3.8 mm . The cell wall length is $l = d / \sqrt{3}$ and d is the cell diameter.
- The relative density of the foam is taken as 9% or 0.09 .

For the yield strain of the solid material in the foam, the yield strain of AA1050 is taken. This value is 38% , see appendix 4.

In formula (6) the following cyclic analog for the flow curve in the region of uniform plastic deformation is used:

$$\Delta\sigma = K'(\varepsilon_p)^{n'} \quad (10)$$

In the *Beam Bending* model the following cyclic parameters are used:

- The cyclic strength coefficient of AA1050, K' of 200 MPa [45].
- The Coffin-Manson exponent for aluminum alloy 1100 which is $\beta = -c = 0.69$ [33].
- The cyclic strain hardening exponent of $n' = 0.09$. This is based on a cyclic strain hardening exponent for aluminum alloy 2024 of $n' = 0.09$ [33] and a cyclic strain hardening exponent for aluminum of $n' = 0.093$ [34].

The micro structural constant $g_\delta = 0.0001433$. This value was fitted on the following experimental data points, an FCG velocity of $da^*/dN = 10^{-9} \text{ m/cycle}$ at $\Delta K = 0.095 \text{ MPa}\sqrt{\text{m}}$ and a $da^*/dN = 10^{-7} \text{ m/cycle}$ at $\Delta K = 0.125 \text{ MPa}\sqrt{\text{m}}$.

Using the data of the FCG curves and the chosen yield strain the Coffin-Manson constant C_2 results in a value of 0.3065 , see formula (7).

The model returns an FCG curve in the Paris region. For the data used, a Paris exponent m of 16.1 is found. In figure 36 this result is shown together with the experimental data in figure 18. The experimentally found Paris exponent is 15.6 .

In the relation of Morrow [30] the a cyclic strain hardening exponent n' and the Coffin-Manson exponent of c are related by the following equation:

$$c = -\beta = \frac{-1}{(1 + 5n')} \quad (11)$$

Morrow [30] relation between the a cyclic strain hardening exponent n' and the Basquin exponent of α are related by the following equation:

$$b = -\alpha = \frac{-n'}{(1 + 5n')} \quad (12)$$

When the relation of Morrow [30] is used, a cyclic strain hardening exponent of $n' = 0.094$ and a Coffin-Manson exponent of $c = 0.680$, result in the a Paris exponent of 15.6 , which is equal to the experimentally found value.

This value of the cyclic strain hardening exponent n' is very close to the value of 0.093 that is given by Matěj [34] for aluminum. Using the relation of Morrow [30] we can determine the cyclic strain hardening exponent n' from the Coffin-Manson exponent c or from the Basquin exponent b . For example Suresh [33] gives for

AA1100 the value $c=-0.69$ for the Coffin-Manson exponent, which results in a $n'=0.09$. Matěj [34] gives for pure aluminum a value $c=-0.61$ for the Coffin-Manson exponent which result in $n'=0.128$.

Both high cycle and low cycle fatigue versions of the *Beam Bending* model must have the same result since the cyclic strain hardening exponent n' is the ratio of the Basquin exponent b and from the Coffin-Manson exponent c [30], see equations 4, 6, 11 and 12.

Generally a lower cyclic strain hardening exponent results in a shorter fatigue life [30] at low cycle fatigue. In the *Beam Bending* model a lower cyclic strain hardening exponent results in a higher FCG rate, table 3.

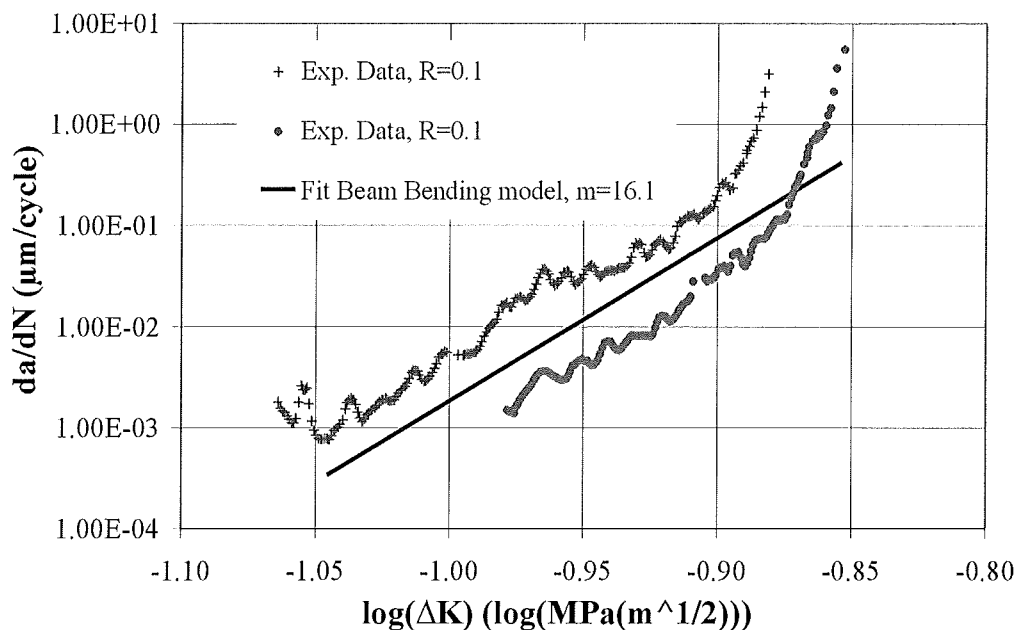


Figure 36 Example of measured Alporas aluminum foam FCG curve at $R=0.1$ and the FCG curve resulting from *Beam Bending* model with a Paris exponent of 16.1

6.5 FCG curve and influence of structure

In the SCEF model the fatigue process in the M(T) sample is assumed to be a series of fatigue processes. During each of those fatigue processes only one cell edge is subjected to fatigue. For each failed cell edge the crack in the sample will grow by a amount that is equal to the cell cross section divided by the thickness of the M(T) sample. This results in an increase of stress intensity each time the crack grows. During a fatigue process in a cell edge the stress intensity is assumed constant, since the increase of the crack length in this cell edge is very small (micro scale) compared to the crack length in the sample (macro scale).

In the simulation of the SCEF model it is assumed that approximately 70% of the mass is present in the cell edges [26]. This is based on the structure of conventional Alporas [10, 19 and 26]. From this data a spread in the cell edge cross section is created using a random spread around the average cross section of the cells edges.

The fatigue life of a cell edge is assumed to be proportional to ΔK^{-m} . The experimental values for the Paris exponent of 15.6 and the cell diameter of 3.8 mm are used. The constants in the model are adapted so that the model will match the experimental data of figure 18.

The cell edges are sorted in series of cell edges with increasing cross section, see figure 6. This is to simulate a the growth of a more of less straight crack front.

The *Sequential Cell Edge Failure* model results in curves, that have a similar bumpiness as the experimentally found FCG curves, see figure 37.

In figure 37 the measured FCG curves of figure 18 are shown together with the SCEF model and the cross sections of the cell edges that are used in the model. The model clearly shows a decrease in da/dN when the crack encounters a stronger cell edge. This suggests that at each point in the curve the fatigue process is dominated by very few cells and that the cell faces or membranes hardly play a role.

Note. The model returns a smooth curve, if the order of the fatigue processes over the entire sample is sorted according to a single series of increasing cell edge thickness.

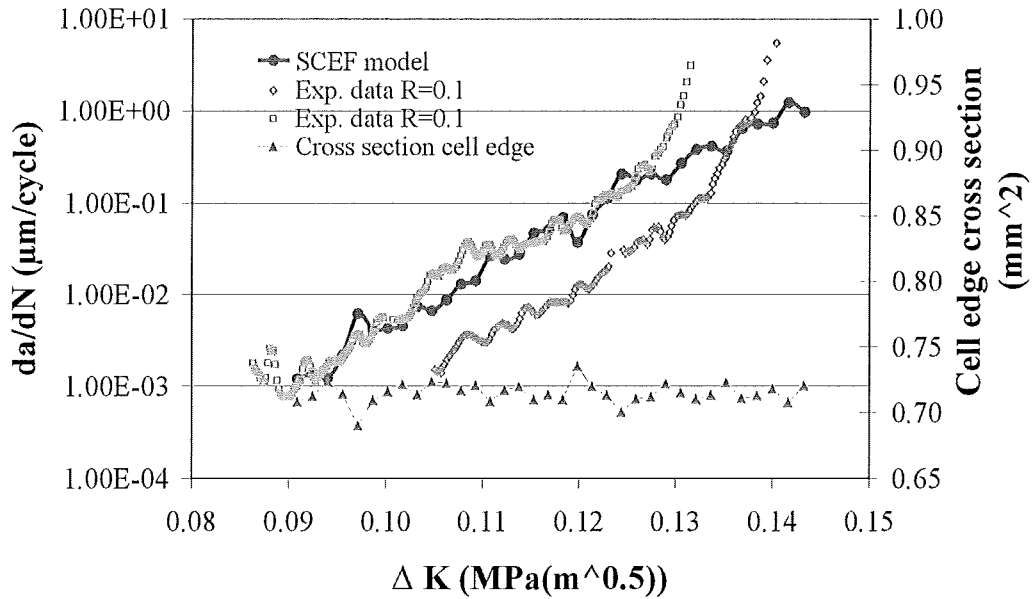


Figure 37 Sequential Cell Edge Failure model.

6.6 Comparison of the crack closure fits

From the crack closure fits it is clear that crack closure plays a role during fatigue in the tested Alporas foam. In the crack closure concept the approaches of *Foam* ΔK and the ΔK approach according to ASTM both seem to work. However in the ΔK approach according to ASTM approach the efficiency of the process seems to increase for negative load ratios, see figure 22. In effect the ΔK approach according to ASTM approach and the *Foam* ΔK approach have the same amount of ΔK available for crack growth. However since the negative ΔK is missing in the ΔK approach according to ASTM approach, the increase in efficiency is a compensation to get the same amount of effective ΔK . This implies that the *Foam* ΔK approach is to be preferred.

In a thought experiment one can assume the maximum load to be constant. In this case the stress intensity in the ΔK approach according to ASTM is constant for negative load ratios while the fit changes.

From figure 22 it is clear that the *Foam* ΔK approach has a higher efficiency than the *Schijve fit* for solid metals, especially in the negative load ratio range. This implies that there is more ΔK available for crack growth in the used metal foam. This is possible when another process is active in the range of the negative ΔK .

6.7 Load mechanisms in foam

During the fatigue process a cell edge will bend at both ends near the cell nodes. This will happen in opposite directions during tensile loading and during compression loading, see figure 2. A tensile surface stress results in the cell edge surface due to both an external tensile load and an external compression load, as is shown in figure 38. These induced surface tension stresses will manifest themselves at different locations on the cell edge. This means that near the cell node fatigue cracks can develop on two sides of the cell edge and that both tensile load and compression load contribute to the crack growth. Note. The crack growth at a specific site will grow, when the induced surface tensile stress is active at that site.

This results in a higher amount of stress intensity available for crack growth and more sites where the cracks can grow.

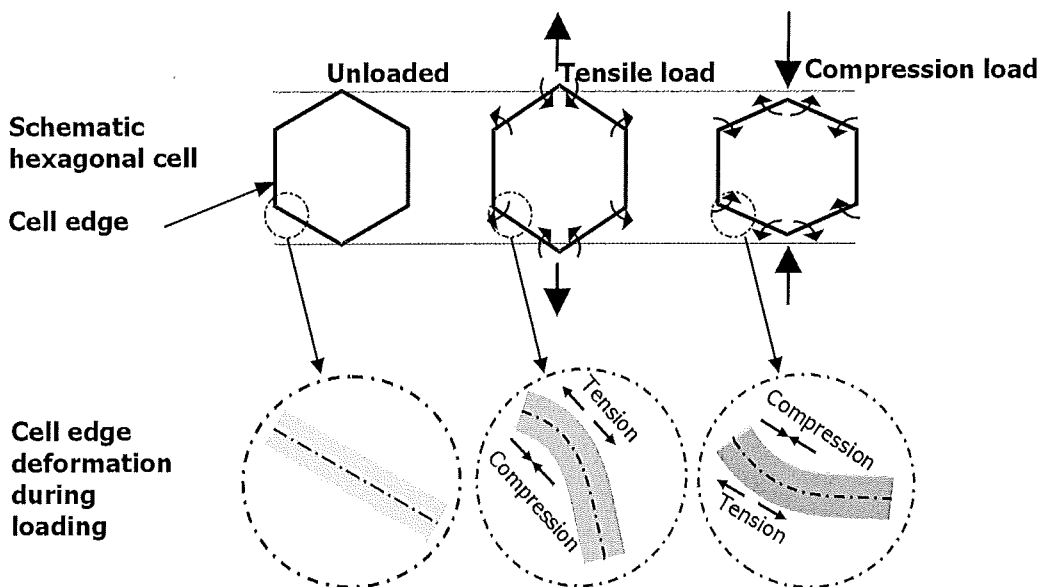


Figure 38 Deformation of cell edges during fatigue loading

6.8 Crack closure fit

A restriction of $a+b+c=1$ was used for the crack closure fit. This assumes that all FCG curves with an $R < 1$ shift are due to crack closure. In some materials [18] there is no shift in the curves with a load ratio $R > 0.8$ and in some cases $R > 0.5$. In these materials another restriction is used. Since it was very difficult to perform FCG experiments at $R=0.7$ or higher, it has not been possible to test this.

6.9 Hardening exponent of Alporas and AA1050

The hardening exponent of Alporas foam is 0.47 and the hardening exponent of annealed AA1050 is 0.44. The last material approaches the material from which Alporas is made. Extrapolation of the values Van Haaften [35] yields a value of 0.41 for annealed AA1050. Compared to the hardening exponent of other metals these values are high, see table 3. All hardening exponent values are determined from the plastic deformation region of more or less the same material.

In foams the plastic deformation is generally localized. This means that the hardening exponent is determined at the plastic deformation of only a few cells or cell edges. The material from which these cells are made is subjected to strain hardening. The other cells in the sample take no part in this process. Under these circumstances the composition of the material from which the foam is made is dominant for the strain hardening of the foam.

Since the values of the hardening exponents are greater than 0.15, cyclic strain hardening is expected [30 and 36]. The ratio of the monotonic ultimate tensile strength and the 0.2 percent offset yield strength is greater than 1.4. In this situation cyclic strain hardening is also expected [30 and 36].

7 Conclusions

The Alporas closed cell aluminum foam has a rather high Paris exponent, which is about five times the Paris exponent of a solid aluminum alloy. The stable crack growth region or Paris region is at low ΔK values compared to solid metals. This makes the material less suitable for applications where failure predictions are necessary.

The Paris exponent is influenced by the free surface when the M(T)-sample thickness is below 35 mm. This explains the difference between the experimentally found Paris exponents and values reported in literature.

The failure mode of the fatigue fracture surfaces is ductile with evidence of slip and plastic deformation.

A novel form of crack closure does occur in the Alporas aluminum foam during FCG. It is hypothesized that the structure of the foam transforms macro compression loads into surface tension loads on a micro scale. Thus enlarging the effective load available for FCG. This hypothesis needs further verification.

The part of the spread in the results that is caused by material variation is at least 40% of the spread in the experimental results on the standard samples.

The used method of FCG measurement is of limited use for measuring the initiation stage of the crack growth. The experiments show a micro-crack like inhibition effect at the low end of the Paris region. The possible influences of micro-cracking, defects and inclusions need further investigation.

It is demonstrated that the *Beam Bending* model is capable of predicting the FCG curve, by using material parameters. There is a good agreement between the model and the experimental data.

The low cyclic strain hardening exponent of the Alporas foam results in the occurrence of cyclic strain hardening and a high Paris exponent. This has a negative effect on the fatigue life.

It has been demonstrated that the SCEF model can simulate the bumpiness of the foam FCG curves as a result in a variation in cell edge thickness. This demonstrates the influence of the local structure on the fatigue process in foam.

References

- [1] Ashby M.F., Evans A., Fleck N.A., Gibson L.J., Hutchinson J.W., Wadley H.N.G. Metal foams; A design guide. Butterworth-Heinemann, 1st ed. (2000).
- [2] Hans-Peter Degischer Brigitte Kriszt Handbook of cellular Metals Production, Processing, Applications. Wiley-VCH 2002
- [3] Geerlofs N. Material properties and fatigue of Aluminum foam. Literature review July 2001.
- [4] Harte A.M., Fleck N.A., Ashby M.F. Fatigue failure of an open cell and a closed cell aluminum alloy foam. *Acta Materialia* 47, (1999), 2511-2524.
- [5] McCullough K.Y.G., Fleck N.A., Ashby M.F. The stress life fatigue behaviour of aluminum alloy foams. *Fatigue & Fracture of Engineering mater Struct*, 23, (2000), 199-208.
- [6] Schulz O., des Ligneris A., Haider O., Starke P. Fatigue behaviour, strength, and failure of aluminum foam. *Advanced Engineering Materials*, 2, (2000), 215-218.
- [7] Sugimura Y., Evans A.G., Harte A.M., Fleck N.A. Compression fatigue of a cellular Al alloy. *Materials Science and Engineering A*, A269, (1999), 38-48.
- [8] Zettl B., Mayer H., Stanzl-Tschegg S.E., Degischer H.P. Fatigue properties of aluminum foams at high numbers of cycles. *Materials Science and Engineering A*, A292, (2000), 1-7.
- [9] Murakami Y., Endo M. Effects of defects, inclusions and inhomogeneities on fatigue strength. *Fatigue*, 16, (1994), 163-182.
- [10] Banhart J., Brinkers W. Fatigue behavior of aluminum foams. *Journal of Material Science Letters* 18 (1999) 617-619.
- [11] Harte A.-M., Fleck N.A., Ashby M.F.; The fatigue strength of sandwich beams with Aluminium foam core. *International Journal of Fatigue* 23 (2001) 499-507.
- [12] Ohrndorf A., Krupp U., Christ H.-J. Fatigue behaviour of open- and closed-cell Al-foams. Presentation at Metfoam 2001.
- [13] Shipsha A., Burman M., Zenkert D. On mode I fatigue crack growth in foam core materials for sandwich structures. *Journal of sandwich structures and materials*, vol 2 April 2000 103-116.
- [14] Zettl B., Mayer H., Stanzl-Tschegg S.E. Fatigue properties of Al-1Mg-0.6Si foam at low and ultrasonic frequencies. *International Journal of Fatigue* 23 (2001) 565-573.
- [15] Olurin O.B., McCollough K.Y.G., Fleck N.A., Ashby M.F. Fatigue crack propagation in Aluminium alloy foams. *International Journal of Fatigue* 23 (2001) 375-382.
- [16] Gibson LJ, Ashby MF. Cellular solid: structures and properties. 2nd ed. Cambridge: Cambridge University Press, 1997.
- [17] Huang J.S., Lin J.Y. Fatigue of cellular materials. *Acta Materialia*, 44, (1996), 289-296.
- [18] M. Janssen, J. Zuidema, R.J.H. Wanhill. *Fracture Mechanics*. Delft University Press, 2nd edition 2002.
- [19] Miyoshi T., Itoh M., Mukai T., Kanahashi H., Kohzu H., Tanabe S., Higashi K. Enhancement of energy absorption in a closed-cell aluminum by the modification of cellular structures. *Scripta Materialia*, Vol 41, No 10, pp. 1055-1060, 1999.

-
- [20] Mukai T., Kanahashi H., Miyoshi T., Mabuchi M., Nieg T.G., Higashi K. Experimental study of energy absorption in a closed-cell foam under dynamic loading. *Scripta Materialia*, Vol 40, No 8, pp. 921-927, 1999
- [21] Huang J.S., Shi-Yi Liu. Fatigue of isotropic open cell foams under multiaxial loads. *International Journal of Fatigue*, 23, (2001), 233-240.
- [22] Bart-Smith H., Bastawros A.F., Mumm D.R., Evans A.G., Sypeck D.J., Wadley H.N.G. Compressive deformation and yielding mechanisms in cellular Al alloys determined using x-ray tomography and surface strain mapping. *Acta Materialia*, **46**, (1998), 3583-3592.
- [23] Bastawros A.F., Bart-Smith H., Evans A.G. Experimental analysis of deformation mechanisms in a closed cell aluminum alloy foam. *Journal of the Mechanics and Physics of Solids*, **48**, (2000), 301-322.
- [24] Paul A., T. Seshacharyulu, U. Ramamurty. Tensile strength of a closed cell Al foam in the presents of notches and holes. *Scripta Materialia*, **40**, (1999), 809-814.
- [25] McCullough K.Y.G., Fleck N.A., Ashby M.F. Toughness of aluminum alloy foams. *Acta Materialia*, **47**, (1999), 2331-2343.
- [26] Elmoutaouakkail A. Salvo L. 2D and 3D characterisation of metal foam using X-ray tomography, Conference proceedings Metfoam2001.
- [27] Sugimura Y., Meyer J., He M.Y., Bart-Smith H., Grenstedt J., Evans A.G. On the mechanical performance of closed cell Al alloys foam. *Acta Materialia*, **47**, (1997), 5245-5259.
- [28] Motz C., Pipan R. Fracture behaviour and fracture toughness of ductile closed-cell metallic foams. *Acta Materialia*, **50** (2002) 2013-2033.
- [29] Phillips R.A., King J.E., Moon J.R. Fatigue crack propagation in some PM steels. *Powder Metallurgy 2000* vol 43 no 2 149-156.
- [30] Dieter G.E. *Mechanical Metallurgy*. McGraw-Hill Book Company SI Metric Edition 1988.
- [31] Schijve J. *Fatigue of Structures and Materials*. Kluwer Academic Publishers 2001
- [32] ASTM E 647-00 Standard Test Method for Measurement of Fatigue Crack Growth Rates; (2000)
- [33] Suresh S. *Fatigue of materials*. Cambridge University Press 2nd ed 1998.
- [34] Matěj Bělý, *Material Science Monographs 78; Cyclic Deformation and Fatigue of Metals*. Elsevier, 1993.
- [35] W.M. van Haften, *Constitutive behaviour and hot tearing during aluminium DC casting*. PhD Thesis, 2002.
- [36] Richard W. Hertzberg, *Deformation and fracture mechanics of engineering materials*. Fourth edition. John Wiley & Sons, 1996.
- [37] Miyoshi T., Itoh M., Akiyama S., Kitahara A. Alporas aluminum foam: Production process, properties and applications. *Advanced engineering materials* 2000, 2, No 4, 179-183.
- [38] Voort G.F.van der; *Applied metallography*. Van Nostrand Reinhold company, New York, 1986.
- [39] ASTM E 8-00b Standard test methods for Tension Testing of Metallic Materials; (2000)
- [40] ASTM E 646-00 Standard Test Method for Tensile Strain-Hardening Exponents (n-Values) of Metallic Sheet Materials; (2000)

- [41] Andrews E.W., Gioux G., Onck P., Gibson L.J. Size effects in ductile cellular solids. Part II: experimental results. *International Journal of Mechanical Sciences*, **43**, (2001), 701-713.
- [42] Ament P.C.H. Crack Length Measurement with the Potential Drop Method. Literature review September 1996.
- [43] Leonard C. Feldman, James W. May Fundamentals of surface and thin film analysis, PTR Prentice Hall (1986)
- [44] J. Zuidema; Current work on FCG of aluminum alloys. 2003
- [45] CHR. Boller, T. Seeger Materials data for cyclic loading; Part D: Aluminium and Titanium alloys. Elsevier Amsterdam (1987)
- [46] www.matweb.com
- [47] Metals Handbook, Vol.2 - Properties and Selection: Nonferrous Alloys and special-Purpose Materials, ASM International 10th Ed. 1990.
- [48] Fleck N.A., Olurin O.B., Chen C., Ashby M.F. The effect of hole size upon the strength of metallic and polymeric foams. *Journal of the Mechanics and Physics of solids* 49 (2001) 2015-2030.

Appendix

Appendix 1: Settings X-ray spectrometer

Spectrometer	Philips PW1480
Röntgen tube	Rh (6kV)
Analyze crystal	LiF220
Acceleration voltage	40kV
Current	60mA

Appendix 2: Composition of aluminum alloy 1050

Composition of aluminum alloy 1050, www.matweb.com [46]	
Element	Wt%
Al	Min 99.5
Cu	Max 0.05
Fe	Max 0.4
Mg	Max 0.05
Mn	Max 0.05
Si	Max 0.25
Ti	Max 0.03
V	Max 0.05
Zn	Max 0.05

Appendix 3: Settings of Howden pulsed D.C. crack length measuring system

Standard settings of Howden pulsed D.C. crack length measuring system, INVnr.71880321	
Current	15A
Gain x	2
Gain y	2
Stored signal	10x/y
Pulse divider	5

Appendix 4: Physical Properties; Aluminum alloy 1050

Physical Properties; Aluminum alloy 1050, Metals Handbook, Vol.2 - Properties and Selection: Nonferrous Alloys and Special-Purpose Materials, ASM International 10th Ed. 1990. [47]		
Property		Remark
Density	2.705 g/cc	
Hardness, Brinell 1050-O	21	500 kg load with 10 mm ball. Calculated value.
Tensile Strength, Ultimate	76 MPa	
Tensile Strength, Yield	28 MPa	
Elongation at Break	39 %	In 5 cm; Sample 1.6 mm thick
Modulus of Elasticity	69 GPa	In Tension
Poisson's Ratio	0.330	
Shear Modulus	26 GPa	Estimated from similar Al alloys.
Shear Strength	51 MPa	Calculated value.
Compressive Modulus	70.4 GPa	Estimated from tensile modulus
Melting Point	646 - 657 °C	
Solidus	646 °C	
Liquidus	657 °C	

Appendix 5: Properties Alporas foam of 11% density.

Alporas foam of 11% density [48].		
Property		Remark
E	0.34 (GPa)	Elastic
ν	0.2	Elastic
ϵ_y	0.45%	
σ_{UTS}	1.53 (MPa)	
strain hardening exp. n	0.15	n>0.15 hardening n<0.15 softening
α	1.8	ratio of the elliptical yield surface of the von Mises stress σ_e
J_{IC}	1.55 (kJ/m ²)	cell size
l	3.5 (mm)	Cell wall length

